2013-07-02

Capillary Filling of Large Aspect Ratio Channels With Varying Wall Spacing

Dallin B. Murray
Brigham Young University - Provo

Capillary Filling of Large Aspect Ratio Channels with Varying Wall Spacing

Dallin Murray

A thesis submitted to the faculty of
Brigham Young University
in partial fulfillment of the requirements for the degree of

Master of Science

R. Daniel Maynes, Chair
Aaron R. Hawkins
Scott L. Thomson

Department of Mechanical Engineering

Brigham Young University

July 2013

ABSTRACT

Capillary Filling of Large Aspect Ratio Channels
with Varying Wall Spacing

Dallin Murray
Department of Mechanical Engineering, BYU
Master of Science

Quantification and prediction of capillary fluid flow in planar nanochannels is essential to the development of many emerging nanofluidic technologies. Planar nanochannels are typically produced using the standard nanofabrication processes of thermal bonding or sacrificial etching. Both approaches may yield nanochannels that are bowed and/or exhibit non-uniform (i.e. non-planar) wall spacing. These variations in wall spacing affect the transient dynamics of a liquid plug filling the nanochannel, causing deviations from the classical behavior in a parallel-plate channel as described by the Washburn model. Non uniform wall spacing impacts the overall frictional resistance and influences the meniscus curvature. In this thesis, a new analytical model that predicts the meniscus location over time in micro- and nanochannels as a function of channel height was compared to experimental filling data of well-characterized channels with different heights. The wall-to-wall spacing of the utilized nanochannels exhibited height variations between 60 and 300 nm. The model was also validated with microscale channels that were fabricated with a linear variation in the wall-to-wall spacing from 100 μm to 400 μm. The filling speed and meniscus shape during the filling process were determined by dynamic imaging of the meniscus front for several different liquids. A modified Washburn equation that utilizes an effective channel height to predict the filling speed corresponding to the location of the tallest height within a channel was derived. A model was also developed to predict the meniscus distortion encountered in a non-constant height channel, provided the cross-sectional channel heights and the distance from the channel entrance are known. The models developed herein account for induced transverse pressure gradients created by non-constant channel heights. The models are compared to experimental data derived from both nanoscale and microscale channels with good qualitative agreement. These results demonstrate that the capillary flow in nanochannels with non-parallel-plate, linear tapered, or parabolic cross sections can be predicted.

Keywords: capillary, microchannel, nanochannel, parabolic, linear, parallel, effective height, Washburn, modified, non-uniform

ACKNOWLEDGEMENTS

I am especially grateful to Mikell for her support through thick and thin that has allowed this thesis to be written. I am grateful to Kenna and Elsa for each early morning motivational speech. I am also extremely grateful to Dr. Maynes for his patience and magnificent teaching, and to Mark Hamblin for the nanochannels he created for this experimental work.

TABLE OF CONTENTS

LIST OF TABLES

LIST OF FIGURES

1 INTRODUCTION

Micro- and nanofluidics has applicability in many emerging technologies and is a rapidly growing field of scientific research. Characterizing flow through micro- and nanochannels is integral to the development of miniaturized biomedical diagnostic devices, commonly referred to as Lab-on-a-Chip systems. While microfluidic-based chips have been investigated since the early 1990's, commercial implementation has been lacking due to comparable capillary-based analysis methods. Capillary technology is limited at the nanoscale; therefore, nanofluidic microchips should flourish in the experimental space requiring nanoscale channels, such as the separation and segregation of DNA, proteins, or viruses [1,2,3].

Nanochannel technology is limited by the uncertainty in channel heights created by current fabrication processes and the known variability regarding published meniscus filling speed data. Currently manufacturing methods for nanochannels are limited to two well-known processes, thermal bonding and sacrificial etching, with either silicon dioxide wafers or polydimethylsiloxane (PDMS), depending on the intent of the fabricated channels. Both methods are able to achieve large width to height ratios, known as the aspect ratio (W/H). The channels created with these methods may have a width that is orders of magnitude larger than the height and allow an observer to track the meniscus for the full length of the channel. The actual meniscus location can be tracked via camera and compared to the Washburn theory. The Washburn equation allows the meniscus location to be predicted over time for a given liquid

introduced into a large aspect ratio micro- or nanochannel of constant height. Published data on thermally bonded channels with heights larger than 100 nanometers typically remain close to theoretical values; however, for channel heights less than 100 nanometers, the deviation from the Washburn theory grows as the height decreases. The Washburn equation uses the physical properties of the liquid and the channel (i.e. surface tension, bulk viscosity, channel height, and contact angle, or the angle that is measured when the liquid comes in contact with a material) to predict the meniscus location as a function of time for a given liquid introduced into a nanochannel. Difficulties associated with quantifying the variation of channel heights and a lack of post-fabrication measurement data have heretofore prevented the investigation of whether these discrepancies may actually be a result of imperfections within the nanochannels.

In order to quantify and understand the experimental discrepancies with the Washburn equation, each variable believed to cause this deviation from theory must be investigated. A review of the literature reveals that deviations seem to be manifest solely in nanochannel experiments and that the influence of channel height on the Washburn equation at the nanochannel level, specifically when the top and bottom channel walls are not parallel has not been explored previously. The aim of this thesis is to study the effect of variations in the channel height on the Washburn equation in more experimental detail and to understand its contribution to the uncertainty that is encountered between theory and lab results.

The large forces associated with nanofluidic flow have the potential to deform the channel depending upon the material from which it was constructed. Silicon dioxide, a typical bottom and sidewall channel material, is robust enough to withstand the large pressure forces that are present in micro- and nanoscale channels. PDMS is a more flexible material that deforms under pressure. Large capillary forces are prominent in nanochannels due to the large surface-to-

volume ratio. The pressure jump across a liquid-air interface in a parallel-plate nanochannel is $\Delta P = 2\sigma\cos\theta/h$, where σ is the liquid surface tension in air, θ is the advancing dynamic contact angle of the liquid, and h is the distance between channel walls [4]. Consequently, for a liquid plug in a nanochannel surrounded by air, a large negative pressure exists in the liquid phase. For water ($\sigma \approx 72$ mN/m) moving through a hydrophilic channel of $h = 20$ nm and $\theta \approx 40°$ the capillary pressure is nominally 50 bar. Cavitation of the channel surfaces was once of concern; however, the absence of cavitation has since been explained by the height of the channel being smaller than the critical size needed for a liquid vapor bubble to expand and form [5].

A common experimental set up for exploring the liquid filling of nanochannels driven by capillarity is illustrated in Fig. 1 [5-10]. For this relatively simple scenario, comparison to the Washburn model has been performed to yield a measure of the overall resistance to liquid flow [11]. The liquid plug is fed into the channels via a reservoir. The end opposite to the feed reservoir is an empty reservoir that is vented to atmospheric pressure. If this end is capped, the liquid plug will fill as normal but will stop once equalization in pressure between the liquid and the air trapped in the channel has occurred. For the parallel-plate channel, the Washburn equation may be expressed as:

$$\boldsymbol{L = \sqrt{\frac{8t\sigma h\cos(\theta)C}{3\mu}}} \qquad (1)$$

Here L is the length of the moving liquid plug (measured from channel entrance to meniscus location), t represents the elapsed time, and μ is the bulk liquid viscosity. The coefficient C is the Poiseuille number (geometry dependent) and is a measure of the overall frictional resistance in the channel. Simply stated, the meniscus location is proportional to the square root of time multiplied by a constant that is comprised of the variables described above. Note that Eq. 1 is only valid for channels with uniform wall-to-wall spacing. If the channel spacing is not uniform,

Eq. 1 will not predict the correct filling speed. For consistency, the transverse direction is perpendicular to the streamwise direction and parallel to the channel width. The streamwise direction is parallel to the flow direction and perpendicular to the width and height directions.

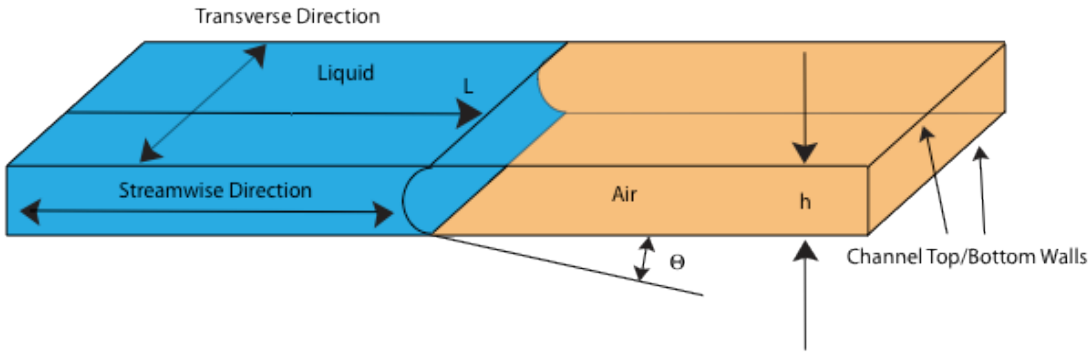

Figure 1: Washburn variable definitions defined

1.1 Review of Recent Literature on Capillary Filling in Nanochannels

There have recently appeared in the literature a number of experimental studies of nanofluidic flow in planar channels, each with a different explanation for the observed conflict between their results and the Washburn equation. At the microscale (channel height > 1 μm), it is well established that classical Stokes flow prevails for a liquid [12] and that $C = 24$ for the parallel-plate channel [13]. By measurement of L, t, h, μ, and θ in the nanofluidic device, the Poiseuille number may be determined from the Washburn expression and compared to the classical value of 24. Literature results uniformly report an increase in C above 24 for liquid flow in nanochannels [5-8]. The deviation has been observed to increase as the nanochannel wall-to-wall spacing decreases, with increases of 25% [7], 40% [6] and 160% [5] reported for flow

through nanochannels of h = 50 nm, 40 nm, and 10 nm, respectively. Tas and coworkers [6] attributed the deviation increase to the electro-viscous influence. However, subsequent analysis suggests that the electro-viscous influence is much too small to account for the observations [12]. Thamdrup and colleagues [13] suggested that the behavior may be due to bubble formation caused by rapid filling; however, bubbles were not seen or mentioned in every channel tested [5-8]. It has been suggested that the enhanced resistance may be due to a local increase in the liquid viscosity due to a molecular layering near the wall [9], though others have reported no such layering in similar-sized channels [14]. It has also been speculated that the adsorption of a film on the dry surface in front of the meniscus affects θ and is manifest as an increase in the overall frictional resistance [7].

Deformation of the nanochannel is another potential explanation for the experimental results. A slight collapse or bowing of channel walls is possible considering the large negative pressures created at the liquid-air interface. The collapse of a channel wall would also manifest itself as an observed increase in the flow resistance.

Honschoten and coworkers [15-17] formulated a modified Washburn coefficient to characterize filling speeds in deformable channels with dynamic wall deflection occurring in the transverse and streamwise directions due to a thin flexible PDMS membrane bonded to the top of the glass substrates. The experiments showed a deformed meniscus front due to the collapse of the channel ceiling; however, the channel surface would only transiently bow as the meniscus proceeded through the channel. A correlation was devised according to the bonded polymer channel ceiling material properties, but no other model was proposed to show the effective change to the Washburn equation according to either a dynamically changing channel geometry or an intrinsically unchanged channel geometry.

Tas et al. [18] related negative pressure gradients to the channel material properties in order to express the deflection in terms of the pressure field for a liquid plug. The static liquid plug exhibited a deformed meniscus due to the collapsed channel ceiling center at both the leading and trailing ends of the liquid plug. The derived correlation relates the exhibited meniscus radii of curvature to the pressure created in the liquid plug, without neglecting wall effects.

Zhu and colleagues [20] related various deviations from the expected Washburn model in thermally bonded PDMS planar microchannels with 90 degree corners, including separate experiments with rounded corners to illustrate the shape of the meniscus front as the corner geometry changes. They noted a deviation between the static and dynamic contact angle as it relates to the negative pressure gradient in a forward moving meniscus flow. They explained that the flow moves forward, with a negative pressure gradient, due to a deviation in the microscale static contact angle while traveling through the nanoscale channels.

1.2 **Fabrication Influence on Contact Angle**

Thermal bonding techniques are commonly employed to create planar nanochannels. Thermal bonding creates channels with three surfaces of the same type of material, which is typically silicon due to the manufacturing constraints in achieving nanoscale height components, and a top surface made from a thermally grown silicon dioxide wafer. The top surface, created from a planar layer of material, is thermally bonded onto the top of the existing saw tooth profiled channel or channels. The top surface is heated just below the melting point of the material, and the material is placed on top of the channel profiles. The resulting channels are then ready for experimentation. However, the planar geometry must be heated close to the melting temperature to complete the bonding process, allowing the material to deform as the

silicon dioxide has already passed its glass transition temperature and potentially changing the height and shape of the channel. A schematic of a thermally bonded nanochannel is shown in Fig. 2. The top thickness in Fig. 2 must be measured before and after thermal bonding to obtain a true measure of the channel height.

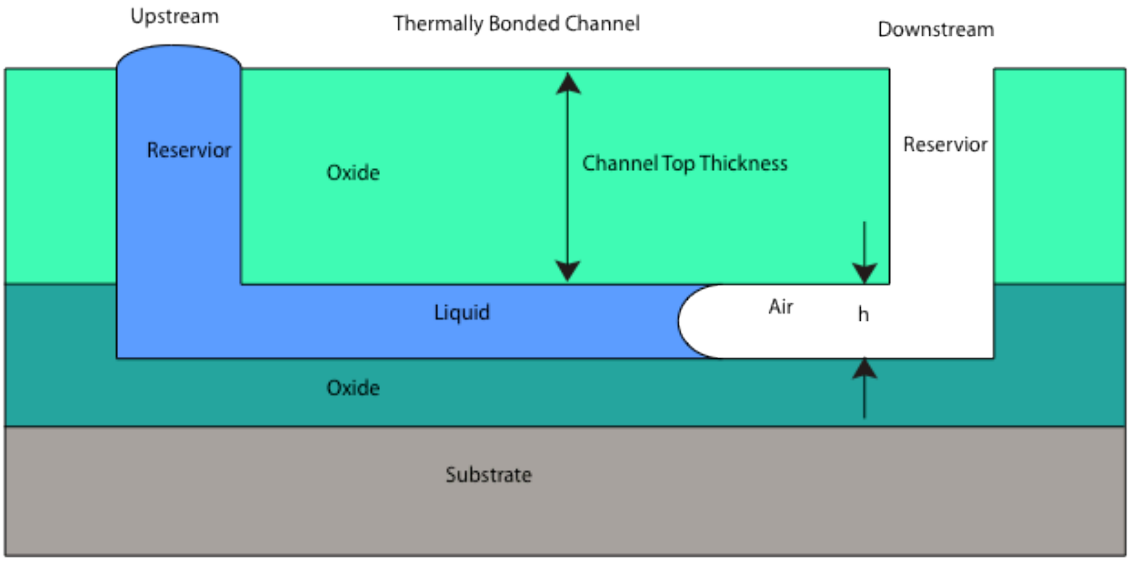

Figure 2: Thermally bonded channel schematic

A lack of scanning electron microscope data or profilometer measurements to quantify the post fabrication channel geometry created from thermally bonded nanochannels complicates interpretation of experimental results from the literature. The height of the channel is a key parameter in the Washburn equation. Without characterizing the actual height of the experimental channels after the thermal bonding process, most experimental investigations fail to show how planar the created geometry remains. Also, the contact angles from the thermal bonded silicon dioxide have not been characterized or correlated to the base silicon material, which could lead to different surface energy or overall flow characteristics between the four channel walls.

Sacrificial etching is an alternative manufacturing strategy to thermal bonding for nanochannels with reduced potential for deformation during production and bowing during filling. Instead of channels created by heating the glass near the melting point and pressing the channel pieces together, a sacrificial material is used to create the channel characteristics. Hamblin and coworkers [21] used sacrificial etching techniques to create nanochannels with step changes in the height of varying sizes. The cross section of a channel produced using sacrificial etching is comprised completely of rigid silicon dioxide walls instead of two different materials as shown in the thermally bonded schematic (Fig. 2). Channel bowing is defined as bowing either up or down in the center unless a linear taper is specifically mentioned. The edges connected to the sidewalls do not deflect. The channel sidewalls and the channel bottom wall do not deflect due to the substantial amount of material thickness behind the side and bottom walls. Increasing the channel top thickness can decrease the amount of bowing encountered during the channel filling. The sacrificial etching method can also be employed to furnish channels of varying top thickness to allow deflection or bowing, without having to create geometry with two different types of glass. Thus, the issues of heating glass near its melting point and joining of dissimilar materials is avoided, simplifying channel height measurements. Sacrificially etched channels increase confidence in the final experiments and correlations because the contact angles are the same on all walls.

For both types of nanochannel fabrication methods (thermal bonding or sacrificially etched channels) bowing of the channel walls may exist. This non-uniform spacing may result from intentional actions or it may be unintentional. However, the non-uniformity of the channel cross section directly impacts filling and meniscus curvature. The channel top thickness can be designed to induce bowing in the channel top when acted on by the large negative pressure that

exists in the liquid plug. It should be noted channel bowing can manifest itself as an observed increase or decrease in the flow resistance depending on the amount of concave or convex bowing. Further, non-uniform channel wall spacing yields a dynamic meniscus that is curved in the transverse direction. The meniscus curvature also changes shape according to the position downstream from the channel inlet.

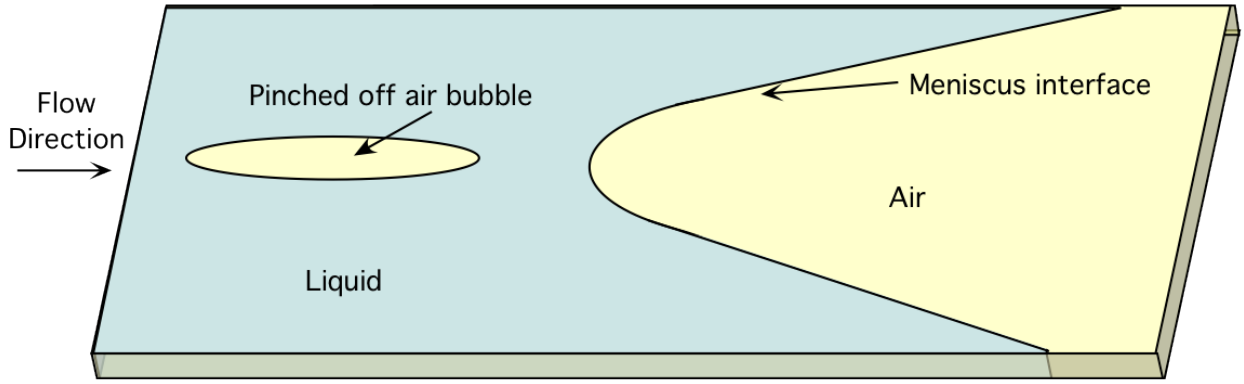

Figure 3: A curved meniscus exists when the wall-to-wall height varies in a concave manner. Parallel-plate channels exhibit a flat meniscus that remains parallel to the channel entrance throughout filling.

The meniscus front becomes deformed when the top center bows upward as illustrated in Fig. 3. The amount of meniscus bowing is determined primarily by the height difference. If the channel walls are under certain severe conditions, vapor bubbles may become entrained in the moving liquid. Experimentation in numerous nanometer scale channels exhibiting thin top walls, which induce bowing, showed a deformed meniscus that extended nearly one third of the channel length beyond the center meniscus location. The non-constant channel height effectively drives a low pressure area at the lowest channel heights creating a favorable flow path for the filling liquid. Previous investigations have not quantified the influence of wall bowing on filling speed dynamics.

1.3 **Focus of Present Investigation**

The focus of this work is to explore both experimentally and analytically the influence of variations in channel wall spacing on capillary filling speeds and meniscus curvature. Two analytical models are developed. The first is essentially a modified Washburn equation that can be used for non-uniform channels to predict filling speed of a meniscus front. The second model is one that describes the dynamic curvature in the meniscus front. These models are developed following classical viscous flow methods. Further, experiments are conducted in both microscale and nanoscale channels to validate the model and to characterize the influence of varying wall spacing on the shape of the curved meniscus during the filling process. Hamblin provided the nanoscale parabolic and nanoscale parallel-plate channels created with various sacrificial metals [21]. Experimentation was devised to show the gradual advance or retreat of a liquid meniscus as a function of channel cross section spacing. The analytical model results are subsequently compared to the nanoscale and microscale experimental tests. The results are applicable to the nanoscale and microscale regime where creeping flow is dominant and the height, width, and length ratios are similar to a nano- or microchannel. The outcomes of this work are:

1) Experimental measurements that quantify filling times and meniscus curvature in both nanoscale and microscale channels with non-uniform channel wall spacing.
2) Two analytical models that predict filling speeds and meniscus curvature for liquids in micro- or nanoscale channels with non-parallel walls.

Overall, channels that exhibit a deformed meniscus exhibit one of two primary flow features. The first is a streamwise motion that can be described by substitution of an appropriately determined effective channel height into the Washburn equation. The second is a

two-dimensional flow pattern, where water flows from the tall sections of the channel to the short sections of channel and yields a curved meniscus front. Though unexpected in the nanochannel regime, the two-dimensional flow pattern was observed and quantified.

Chapter 2 of this thesis develops two analytical models from which filling speeds and local meniscus curvature in channels with varying wall spacing can be determined. Subsequently, Chapter 3 describes the methodology employed in the experiments. Chapter 4 provides the results of the experiments and the theoretical analysis and compares the two. Lastly, Chapter 5 provides conclusions from this work and provides suggestions for future investigations.

2 MODELS FOR PREDICTING FILLING AND MENISCUS DISTORTION IN CHANNELS WITH VARYING CHANNEL HEIGHT

To better understand and predict the filling of nanochannels with varying channel height, two theoretical models were developed. Beginning with the differential form of the momentum equation, the first model was developed to modify the parallel-plate derived Washburn equation. This modified Washburn model allows prediction of the filling time for a liquid meniscus filling a channel with non-constant wall spacing. A second model was developed to predict the meniscus distortion encountered in channels with varying wall spacing. This model was derived from a control volume that evaluates the streamwise pressure gradient created from a non-constant channel height cross-section. The meniscus distortion is then determined as a function of the distance traveled from the entrance of the channel and the ratio of the tallest channel height to the local channel height. In effect, the second model predicts the meniscus location at all heights smaller than the tallest channel height. These models explain why large deviations occur in menisci shapes and filling rates in nanochannels where the constant height Washburn equation fails to correctly predict behavior for channels with a non-constant height.

2.1 Model Development of a Modified Washburn Equation

The modified Washburn equation was derived from the streamwise differential momentum equation by first defining its terms for generic fluid flow and then making assumptions to reduce it to a solvable form. The flow of liquid through a nano- or microscale

channel is described by the streamwise component of the differential momentum, shown in Eq. 2.

$$-\frac{\partial p}{\partial x}+\mu\left(\frac{\partial^2 u}{\partial x^2}+\frac{\partial^2 u}{\partial y^2}+\frac{\partial^2 u}{\partial z^2}\right)=\rho\left(\frac{\partial u}{\partial t}+u\frac{\partial u}{\partial x}+v\frac{\partial u}{\partial y}+w\frac{\partial u}{\partial z}\right)+\rho g_x \quad (2)$$

In Eq. 2, p is the pressure exerted on the fluid, μ is the dynamic viscosity of the fluid, ρ is the density of the fluid, u is the fluid velocity in the streamwise direction, v is the fluid velocity in the transverse direction, w is the fluid velocity in the vertical direction, and g_x is the force of gravity acting in the streamwise direction. y is the vertical direction, z is the transverse direction, x is the streamwise direction, and t is time. We considered steady, laminar flow of a liquid with constant viscosity and density being driven by capillarity through a channel with varying wall-to-wall spacing in the transverse direction, $H(z)$. We also assumed creeping flow where the Reynolds number, a combination of fluid parameters comparing a liquid's inertial forces to its viscous forces, approaches zero. In microscale or nanoscale channel applications, the channel dimensions are such that channel length is much larger than the channel width, and the channel width is much larger than the channel height. In fact, the planar and parabolic bowed nanochannels in this study exhibited a channel length, L, of 1.2 millimeters, with a width, W, of 20 μm ($L/W > 60$), and a wall-to-wall spacing, H, of 100 nm or smaller ($L/H > 12{,}000$).

The differential momentum equation was reduced by employing similarity variables to the Navier-Stokes equation, neglecting terms based on channel geometry, and neglecting other terms based on the flow regime.

A simplified form of the differential momentum equation is obtained after excluding negligible factors. Due to the creeping nature of the flow, fluid advection exercises negligible influence. Further, the width of the channels, W, is very wide compared to H, the channel height,

and consequently $\frac{\partial^2 u}{\partial z^2} \gg \frac{\partial^2 u}{\partial y^2}, \frac{\partial^2 u}{\partial x^2}$. Thus, the streamwise momentum equation reduces to the following (Equation 3).

$$\frac{\partial p}{\partial x} = \mu \frac{\partial^2 u}{\partial y^2} \quad (3)$$

u is the streamwise velocity, P is the local static pressure, and μ is the liquid viscosity. This equation describes the fluid flow within a micro- or nanoscale channel where the shearing stress is balanced by the streamwise pressure gradient.

In order to obtain the velocity of the fluid within the nanochannels, Eq. 3 can be integrated twice subject to two common wall boundary conditions where the fluid at each side wall is at rest. With the conditions that the velocity, u, at $y = 0$ is equal to zero, and the velocity, u, at $y = H$ is equal to zero, the momentum equation is sufficiently constrained to solve for the constants of integration. Doing this yields the local velocity distribution in the liquid phase (Equation 4), where $H(z)$ is the wall-to-wall spacing that varies in the transverse (z) direction.

$$u = \frac{1}{2\mu}\frac{\partial p}{\partial x}(y^2 - H(z)y) \quad (4)$$

The average velocity for the entire channel is found by integrating the local velocity profile over the channel cross-section and dividing by the flow area, A, resulting in Eq. 5.

$$\bar{u} = \frac{-\frac{1}{12\mu}\frac{\partial p}{\partial x}}{A}\int_0^W H^3 dz \quad (5)$$

Solving Eq. 5 for the pressure gradient and substituting back into Eq. 4 allows the velocity distribution to be expressed in terms of the average velocity. Subsequently, the wall shear stress can be written in terms of the average velocity as Equation 6.

$$\tau_w = \mu \left.\frac{du}{dy}\right|_{y=0} = \frac{-6\bar{u}\mu A}{\int_0^W H^3 dz}(-H) = \frac{6\bar{u}\mu AH}{\int_0^W H^3 dz} \quad (6)$$

Next, the pressure jump across the meniscus interface is defined in order to obtain a global force balance to determine how the non-constant channel height affects the Washburn equation. The pressure jump across the meniscus interface can be determined by the Laplace-Young equation (Eq. 7) at any point as

$$\Delta \boldsymbol{P} = \boldsymbol{\sigma}\left(\frac{\mathbf{1}}{\boldsymbol{R_1}} + \frac{\mathbf{1}}{\boldsymbol{R_2}}\right) \quad \textbf{(7)}$$

where R_1 and R_2 are the two local radii of curvature of the meniscus in the streamwise and transverse directions respectively, and σ is the liquid surface tension. R_2 is several orders of magnitude larger than R_1, so the term $1/R_2$ is neglected. R_1 is equal to $\frac{H}{2\cos(\theta)}$ where θ is the liquid-solid contact angle, and the pressure jump across the meniscus at any point is shown in Eq. 8.

$$\Delta \boldsymbol{P} = \frac{\boldsymbol{2\sigma cos(\theta)}}{\boldsymbol{H}} \quad \textbf{(8)}$$

In the case where H is the variable wall-to-wall spacing at the maximum wall-to-wall spacing (Point B), Eq. 8 can be rewritten as Eq. 9.

$$\Delta \boldsymbol{P_B} = \frac{\boldsymbol{2\sigma cos(\theta)}}{\boldsymbol{H_{max}}} \quad \textbf{(9)}$$

Assuming the pressure gradient across the channel in the transverse direction is constant, a force balance can be used to obtain the local meniscus position. As in all duct flows, the pressure across the entire transverse width of the channel is constant since there is no streamline curvature, even though the height varies across the transverse plane (Fig. 4).

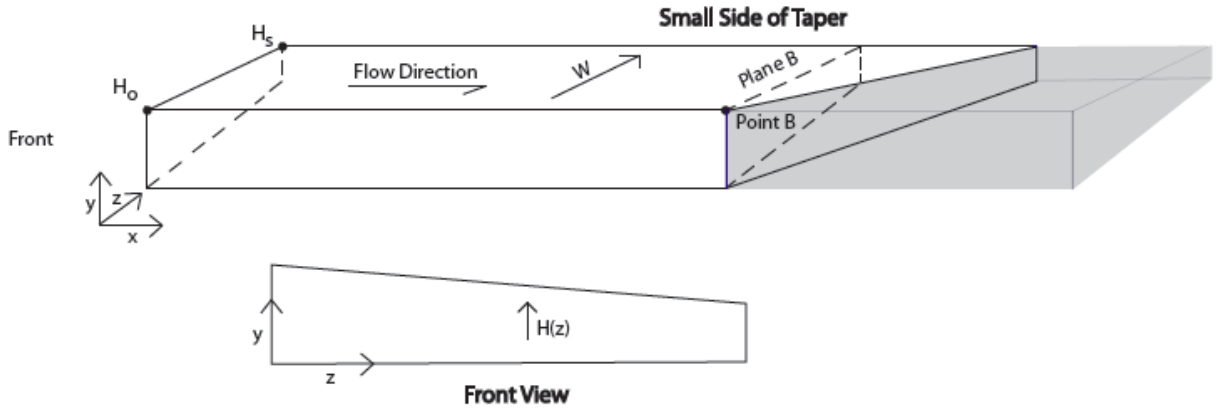

Figure 4: Schematic illustration of a channel with non-constant wall-to-wall spacing. Top provides a side view and the bottom provides a view looking down the channel.

A force balance can be applied to relate the streamwise pressure gradient, local wall shear stress, and pressure jump across the meniscus interface. This force balance requires that the pressure difference between the upstream reservoir and the low pressure generated at the meniscus be balanced by the total frictional resistance along the channel perimeter. Shown in Fig. 5 is an illustration of the meniscus in a channel that extends from the upstream reservoir to the meniscus front. Also shown is a control volume on which the force balance described was performed. This control volume is labeled as Control Volume A and is Δz in width, has a height of H, and a length of L, where L is the distance from the upstream reservoir to point B (plane B). Neglecting resistance to the air motion in front of the liquid plug and noting that there is negligible shear exerted on the lateral edges of the control volume results in Equation 10.

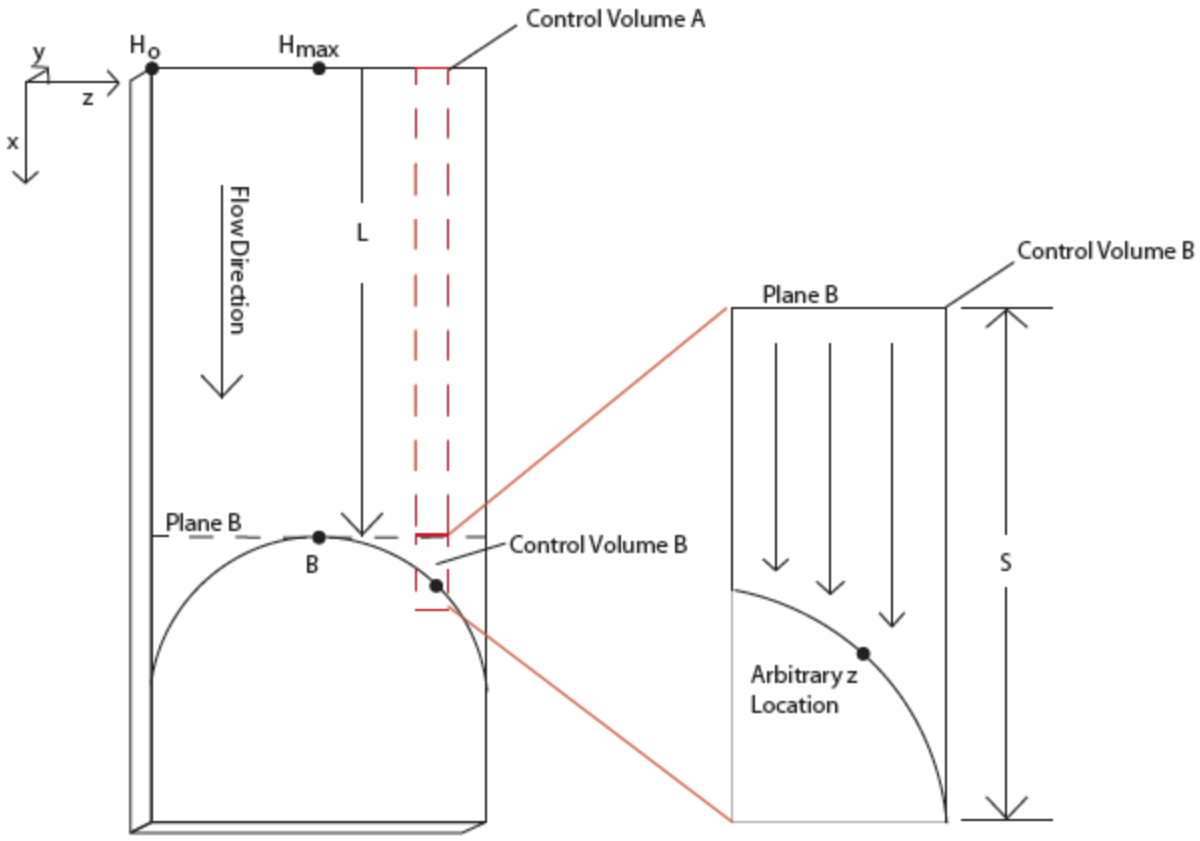

Figure 5: Illustration of the control volume used for analysis. The control volume has a width of Δ*z*, a height of *H*, and a length of *L*.

$$\int_0^L \int_0^W 2\tau_w dz dx = \Delta P_B \int_0^W H dz = L \int_0^W 2\tau_w dz \quad (10)$$

In Eq. 11, L is the length of the liquid plug from the channel inlet to point B, and τ_w is the local wall shear stress. This shear stress varies in the z direction due to the variation in wall-to-wall spacing, although it does not vary in the streamwise direction. ΔP_B is the pressure difference from the upstream reservoir to plane B. Recall that all along plane B the pressure is a constant since there is no local streamline curvature. Simplification of Eq. 11 yields

$$L \int_0^W 2\tau_w dz = \left(\frac{2\sigma cos(\theta)}{H_{max}}\right) \int_0^W H dz \quad (11)$$

Recall the wall shear stress is expressed in terms of the local average velocity in Eq. 6. Substituting the expression for τ_w, from Eq. 6, back into Eq. 11, expressing the average velocity as *dL/dt* and integrating yields Equation 12.

$$\boldsymbol{L_{eff}^{\,2} = \frac{t\sigma cos(\theta) H_{eff}}{3\mu}} \qquad \textbf{(12)}$$

where

$$\boldsymbol{H_{eff} = \frac{\int_0^W H^3 dz}{H_{max} \int_0^W H dz}} \qquad \textbf{(13)}$$

Equation 12 has the appearance of the Washburn equation with two important differences. First, H_{eff} represents an effective channel size, due to varying height across the channel width, rather than a constant wall-to-wall spacing and is evaluated from Eq. 13. Given a specific channel cross section, the integral of Eq. 13 is easily evaluated to determine the effective channel height. Second, the distance determined from Eq. 12 is the length from the channel entrance to the meniscus at the point of maximum channel height (point B. Thus, the modified Washburn equation derived herein (Eq. 12) can be used to calculate the position of the meniscus at the point of maximum channel height (Point B) as a function of time for the filling of a nano- or microchannel with a varying height.

To fully describe fluid flow in a micro- or nanochannel of varying height, the distortion of the meniscus must also be calculated. In other words, the deviation of the meniscus in the region between point B and the meniscus front across the channel must be determined. To model this curvature a force balance is performed on a control volume that extends from the meniscus front to plane B and is denoted as Control Volume B in Fig. 5. For fully-developed duct flows, the streamwise pressure gradient in the liquid is constant if the channel wall-to-wall spacing does not vary in the streamwise direction. It is thus assumed that the pressure gradient is constant

everywhere in the liquid domain, including in the domain $x > L$, where L is distance to the transverse plane B from the channel entrance. At any position along the meniscus front, the pressure difference across the interface is $\Delta P = 2\sigma \cos\theta / H$, where the pressure in the liquid is less than atmospheric pressure by the amount of ΔP. Consequently, the pressure gradient in the liquid is expressed by Eq. 14, where S is the local distance from plane B to the meniscus front in the streamwise direction.

$$\frac{\partial p}{\partial x} = \frac{2\sigma cos(\theta)}{H(L+S)} \quad (14)$$

Recall that the pressure gradient along plane B is a constant. Thus, by evaluating Eq. 14 at point B and at any other point along plane B, an analytical equation for the distortion encountered along the meniscus front is determined. At point B, the length S is zero and at any other location the distance from plane B to the meniscus front is expressed as

$$S = L\left(\frac{H_B}{H(z)} - 1\right) \quad (15)$$

where $H(z)$ denotes the channel height at the meniscus front beyond point B at an arbitrary z location as detailed in Fig. 5.

Equation 15 reveals five important principles. First, the amount of meniscus curvature increases proportionally with increasing distance from the channel inlet. Second, increased deviation from parallel-plate geometry increases variation in the meniscus shape. Third, the amount that the local meniscus position leads the interface at point B is a linear function of the ratio of heights, $H_B/H(z)$. Fourth, it is possible for a meniscus to change dramatically or reverse depending on the local channel wall-to-wall spacing. Fifth, as previously noted, the meniscus curvature is independent of time. All of these trends have been observed qualitatively through experimentation as will be shown in chapter 3.

2.2 Application of the Theoretical Models to Predict Fluid Flow in Non-Planar Nanochannels

Presuming the functional dependence of H on z is known for a channel, Eq. 13 can be evaluated to determine the effective channel height, H_{eff}, for any known non-planar channel geometry. The effective channel heights for a parabolic channel and a linear tapered channel are determined in the following section. With the calculated effective channel height, the modified Washburn equation (Eq. 12) can be used to predict the meniscus location for a non-planar channel. This prediction can be used to understand how the filling rates and meniscus shapes behave in varying height channels.

2.2.1 Parabolic Channel

In this section assumptions and a functional height correlation are presented in order to represent a physical channel's parabolic cross-section with an analytical expression. Channels with a parabolic geometry are smooth, with only one maximum location for convex channels and one minimum location for concave channels. For simplicity, it is assumed that this point occurs at the center of the channel. One obtains Eq. 16 by expressing the height of the parabolic channel based on the width location, W, the maximum channel height, H_{max}, and the channel height at the Cartesian coordinate origin, H_o, shown by the x, y, and z axes in Figures 4 and 5 in section 2.1.

$$\boldsymbol{H = H_o + 4(H_{max} - H_o)\left(\frac{z}{W} - \left(\frac{z}{W}\right)^2\right)} \qquad \textbf{(16)}$$

The effective height of a parabolic channel is determined after integration of the ideal parabolic cross-sectional height profile. As shown in Fig. 4, H_o is the channel height for a parabolic channel near the side walls at $z = 0$ and $z = W$. The maximum channel height at point B is expressed as H_{max}. It is assumed that H_{max} is located at the channel centerline for a parabolic

bowing channel. Using this assumption, the effective channel height, H_{eff}, is solved by integrating Equation 13 and yields Equation 17, which can be calculated solely from the physical properties of any particular channel.

$$\boldsymbol{H_{eff}} = \frac{\frac{H_O H_B}{H_{max}}\left(\frac{3}{7}+\frac{18}{35}\left(\frac{H_B}{H_O}\right)+\frac{24}{35}\left(\frac{H_B}{H_O}\right)^2+\frac{48}{35}\left(\frac{H_B}{H_O}\right)^3\right)}{\frac{H_B}{H_O}+2\left(\frac{H_B}{H_O}\right)^2} \quad \textbf{(17)}$$

For a channel that is convex the height at point B is H_{max} assuming a constant cross section throughout the channel length. Conversely, for a channel bowed down, or concave, $H_o = H_{max}$.

2.2.2 Linear Tapered Channel

For an assumed linearly varying channel, the height profile can be defined according to the transverse distance, z, from the origin. The channel height can be expressed as Eq. 18 assuming a constant cross section throughout the channel length.

$$\boldsymbol{H = H_o + (H_s - H_o)\frac{z}{W}} \quad \textbf{(18)}$$

In Eq. 18 and 19, H_s represents the minimum channel spacing where $z = W$ and was shown in Fig. 4. Substituting Eq. 18 into Eq. 13 and integrating yields the following effective channel height for a linear tapered channel.

$$\boldsymbol{H_{eff}} = \frac{\frac{1}{2}H_s\left(1+\left(\frac{H_O}{H_S}\right)+\left(\frac{H_O}{H_S}\right)^2+\left(\frac{H_O}{H_S}\right)^3\right)}{\frac{H_O}{H_S}+\left(\frac{H_O}{H_S}\right)^2} \quad \textbf{(19)}$$

In Eq. 19, H_{eff} represents the height of the maximum spacing within a channel, where $z = 0$ as defined previously in Fig. 4. This value can be calculated for a given channel and used in the modified Washburn equation to accurately describe the fluid flow.

3 EXPERIMENTAL METHODS

This chapter describes the experimental procedures of determining the fluid constants for the filling experiments with parallel, tapered, and parabolic channels constructed with acrylic or silicon dioxide surfaces for several different liquids. Measurement procedures of fluid specific constants are presented first. Nanoscale and microscale channel specifics, i.e. height measurement and fabrication process, are then described. Next, the meniscus locating algorithm used to process the filling data images is discussed. The resulting fluid constants are used in parallel-plate, parabolic, and tapered filling experiments to compare the classical Washburn model to the modified Washburn model.

3.1 **Fluid Constants**

Surface tension, dynamic viscosity, and advancing contact angle were assumed to be constant for each specific fluid, regardless of the channel shape. The methods used to obtain each fluid constant are provided in this section; however, the results are presented in their respective nanoscale or microscale sections if the constant is applicable to one length scale but not the other. Determination of accurate fluid constants is imperative when comparing the data to the filling theory to develop a complete understanding of meniscus distortion observed in parabolic channels.

3.1.1 Surface Tension Constant

The surface tension constants for methanol, isopropyl alcohol, and deionized water, were determined via static measurement in a vertical channel of known spacing, R. Glass microscope slides separated at constant spacing were placed into the solvent, and a picture was taken after the fluid had reached equilibrium. The image was analyzed in MATLAB to determine the equilibrium fluid height, H_1. The static contact angle, θ_{sta}, was determined using a goniometer (see Section 3.1.2). The specific gravity of the fluid, γ, was adjusted according to fluid temperature. The surface tension, σ, was calculated using Eq. 20. The calculated surface tension values for deionized water, isopropanol, and methanol are found in section 3.1.4.

$$\boldsymbol{\sigma = \frac{H_1 \gamma R}{2cos(\theta_{sta})}} \quad \textbf{(20)}$$

3.1.2 Static and Dynamic Contact Angle Measurements

Static contact angle measurements were taken via a goniometer in order to compute the surface tension of each fluid. Tabulated contact angle values were not employed in this thesis; measurements were made for each material and fluid to ensure accuracy. The goniometer measurements were taken by placing a fluid droplet on the experimental surface and adjusting the eye-piece until the droplet's outline was in focus. The first eye-piece section was rotated until the graduation line aligned with the liquid-solid interface across the entire droplet. The second eye-piece was rotated to match the curvature of the fluid droplet where it met the substrate. The static contact angle was recorded for the right and left sides of the outline to within half of a degree. The right and left contact angles were then averaged to obtain the average static contact angle. This procedure was repeated for each of the three liquids in a matrix fashion across clean experimental surfaces.

3.1.2.1 Microscale Channel Contact Angle Measurement

Static contact angles for three different fluids on acrylic microscale surfaces were determined and are given in Table 1. The goniometer experiments were performed in a matrix fashion across the entire width and length of the channel to maximize the number of measurements (n=12) for a given surface treatment and fluid combination.

Table 1: Static Contact Angles Measured on an Acrylic Substrate

	Methanol	Isopropanol	De-ionized Water
	Degrees	Degrees	Degrees
Average Static Contact Angle	0	0	65.2 ± 2.9

The advancing contact angle for de-ionized water is 43.1% of the measured static contact angle. The values diverge because the static contact angle is a stagnant measurement and the advancing contact angle is derived while the fluid is in motion.

3.1.2.2 Nanochannel Contact Angle Measurement

Nanochannel static contact angles, shown in Table 2, were measured on the external chip surfaces in a matrix fashion to maximize the number of measurements where de-ionized water was the working fluid. It was the only fluid used for comparing flow data with other published work [4, 5, 7, 15, 16, 19, 20, 21]. Three sacrificial cores were used to fabricate nanochannels: aluminum, germanium, and chromium. Each are labeled in abbreviation form in Table 2. Acetic

acid, aqua regia, nanostrip, sulfuric acid, and hydrogen peroxide are commonly used surface treatment solvents in nanochannel fabrication.

Table 2: Static Contact Angle for a Glass Substrate with Aluminum and Germanium and Chromium Cores

	Al & Ge Acetic Acid	Al & Ge Aqua Regia	Al & Ge Nanostrip	Al & Ge Sulfuric Acid	Cr Hydrogen Peroxide
	Degrees	Degrees	Degrees	Degrees	Degrees
Average Static Contact Angle	14 ± 2	18± 2	5 ± 5	8.5 ± 2	8.5 ± 1.5

Advancing contact angles were calculated to compute and compare the classical Washburn equation with the modified Washburn equation. We assumed that the static contact angle is not representative of a flowing liquid. The advancing contact angle of each fluid was determined by plotting the parallel-plate filling data in terms of the square of the meniscus position versus time for the average of three experimental samples. A linear regression of the L^2 versus t data was obtained while setting the y-intercept to zero. The Washburn equation can be rearranged to solve for the advancing contact angle (Eq. 21).

$$\boldsymbol{\theta_{adv} = cos^{-1}\left(\frac{3\mu L^2}{t\sigma h}\right)} \quad \textbf{(21)}$$

Recall that μ is the dynamic viscosity, L, is the location of the meniscus from the entrance, t, is the elapsed time from the fluid entering the channel, H, is the channel height, and σ is the surface tension value for a given fluid. In some instances, calculation of the advancing contact angle, θ_{adv}, from the experimental data resulted in an angle below zero degrees, which is infeasible. In

those cases a value of zero was recorded. The resulting advancing contact angles obtained from parallel-plate micro- and nanoscale experimentation were assumed to be constant regardless of channel geometry. The values used during calculation for all fluids of interest are provided in sections 3.1.4 and 4.1.4.

3.1.3 Dynamic Viscosity

Dynamic viscosity values for each fluid were taken from tabulated values; however, the fluid temperature was obtained to correctly adjust for viscosity variation. The fluid temperature was measured before each experiment with a thermocouple to a precision to 0.5 degrees Celsius. The dynamic viscosity of each fluid was determined by linear interpolation between two tabulated values (Table 3). The tabulated values were taken from material safety datasheets and from textbooks [22-24].

Table 3: Dynamic Viscosity Linear Interpolation Limits

	Lower Limit Temp	Intermediate Limit Temp	Upper Limit Temp	Lower Limit Temp Viscosity	Intermediate Limit Temp Viscosity	Upper Limit Temp Viscosity
	Deg C	Deg C	Deg C	Pa-s	Pa-s	Pa-s
Methanol	20		25	5.9×10^{-4}		5.44×10^{-4}
Isopropanol	15	25	30	2.86×10^{-3}	1.96×10^{-3}	1.77×10^{-3}
Deionized Water	0		100	1.79×10^{-3}		2.8×10^{-4}

3.1.4 Summary of Experimental Constants

Each table in this section provides the measured fluid constant values for use in the classical Washburn and modified Washburn equations in order to compare theoretical results to experimental results. The average surface tension, dynamic viscosity, advancing contact angle, and fluid temperature values obtained for the acrylic parallel-plate microscale channel experiments are provided (Table 4). The surface tension values obtained for deionized water were within 6.1% of the tabulated values. Methanol and isopropanol were within 2.6% and 5.4% of tabulated values. Each tolerance value shown is calculated using a statistical 95% confidence interval (Tables 4-7).

Table 4: Microscale Parallel-Plate Channel Fluid Constant Values

	Surface Tension	Dynamic Viscosity	Advancing Contact Angle	Fluid Temperature
	Nm	Pa-s	Degrees	Degrees C
Methanol	$0.0233 \pm 2\text{x}10^{-4}$	$5.53\text{x}10^{-4}$	0	24
Isopropanol	$0.0208 \pm 6\text{x}10^{-5}$	$2.122\ \text{x}10^{-3}$	0	23.2
Deionized Water	$0.0676 \pm 2\text{x}10^{-3}$	$1.416\ \text{x}10^{-3}$	28.1	24.8

Fluid constant values applicable to acrylic microscale channels with a tapered cross section are reported in Table 5. Advancing contact angles were derived via linear regression of the filling speed data from the parallel-plate experiments then calculated using Eq. 21. Surface tension values remain unchanged from Table 4 as the channel substrate was unchanged.

Table 5: Microscale Linear Tapered Channel Fluid Constant Values

	Surface Tension	Dynamic Viscosity	Advancing Contact Angle	Fluid Temperature
	Nm	Pa-s	Degrees	Degrees C
Methanol	$0.023 \pm 2x10^{-4}$	$5.58x10^{-4}$	0	23.5
Isopropanol	$0.021 \pm 6x10^{-5}$	$2.14x10^{-3}$	0	23
Deionized Water	$0.067 \pm .002$	$1.43x10^{-3}$	28.1	24

Fluid constant values applicable to nanoscale channels with parallel plate cross sections are reported in Table 5. Advancing contact angles were derived via linear regression similar to microscale channels. Each angle was calculated using Eq. 21. In all cases, a sample size of three or greater was used. Each entry is organized by sacrificial metal, channel height, and surface treatment.

Table 6: Nanoscale Parallel-Plate Channel Fluid Constant Values

Material Height – Surface Treatment	Surface Tension	Dynamic Viscosity	Advancing Contact Angle	Fluid Temperature
	Nm	Pa-s	Degrees	Degrees C
Al 19.5 nm - Acetic Acid	Collapsed	Collapsed	Collapsed	Collapsed
Al 19.5 nm - Aqua Regia	$0.067 \pm .002$	$1.443x10^{-3}$	79.8	23
Al 19.5 nm - Nanostrip	$0.067 \pm .002$	$1.443x10^{-3}$	79.9	23
Al 19.5 nm - Sulfuric Acid	$0.067 \pm .002$	$1.443x10^{-3}$	77.8	23.1
Al 55 nm - Acetic Acid	$0.067 \pm .002$	$1.443x10^{-3}$	56.6	23
Al 55 nm - Aqua Regia	$0.067 \pm .002$	$1.443x10^{-3}$	57.1	23
Al 55 nm - Nanostrip	$0.067 \pm .002$	$1.443x10^{-3}$	56.2	23
Al 55 nm - Sulfuric Acid	$0.067 \pm .002$	$1.441x10^{-3}$	58.1	23.1
Al 88.5 nm - Acetic Acid	$0.067 \pm .002$	$1.439x10^{-3}$	39.2	23.2
Al 88.5 nm - Aqua Regia	$0.067 \pm .002$	$1.441x10^{-3}$	48.5	23.1
Al 88.5 nm - Nanostrip	$0.067 \pm .002$	$1.441x10^{-3}$	37.7	23.1
Al 88.5 nm - Sulfuric Acid	$0.067 \pm .002$	$1.441x10^{-3}$	45.0	23.1
Cr 71.5 nm - Nanostrip	$0.067 \pm .002$	$1.443x10^{-3}$	37.4	23
Cr 86.5 nm- Acetic Acid	$0.067 \pm .002$	$1.441x10^{-3}$	24.9	23.1

Table 6: Continued

Material Height – Surface Treatment	Surface Tension	Dynamic Viscosity	Advancing Contact Angle	Fluid Temperature
	Nm	Pa-s	Degrees	Degrees C
Cr 86.5 nm - Aqua Regia	0.067 ± .002	1.443×10^{-3}	17.4	23
Cr 86.5 nm - Nanostrip	0.067 ± .002	1.443×10^{-3}	36.6	23
Cr 86.5 nm - Sulfuric Acid	0.067 ± .002	1.443×10^{-3}	23.4	23
Ge 57 nm - Acetic Acid	0.067 ± .002	1.441×10^{-3}	35.9	23.1
Ge 57 nm- Aqua Regia	0.067 ± .002	1.443×10^{-3}	27.5	23
Ge 57 nm - Nanostrip	0.067 ± .002	1.443×10^{-3}	16.9	23
Ge 57 nm - Sulfuric Acid	0.067 ± .002	1.441×10^{-3}	17.6	23.1
Ge 57 nm - Hydrogen Peroxide	0.067 ± .002	1.443×10^{-3}	36.6	23
Ge 57 nm - 3 μm top	0.067 ± .002	1.443×10^{-3}	53.7	23
Ge 57 nm - 5 μm top	0.067 ± .002	1.443×10^{-3}	16.7	23
Ge 57 nm - 7 μm top	0.067 ± .002	1.443×10^{-3}	18.2	23
Ge 85.5 nm - Acetic Acid	0.067 ± .002	1.443×10^{-3}	45.3	23
Ge 85.5 nm - Aqua Regia	0.067 ± .002	1.441×10^{-3}	28.8	23.1
Ge 85.5 nm - Nanostrip	0.067 ± .002	1.443×10^{-3}	48.5	23
Ge 85.5 nm - Sulfuric Acid	0.067 ± .002	1.441×10^{-3}	47.1	23.1

The averaged fluid constant values used in parabolic nanoscale channel experiments are provided in Table 7. The advancing contact angle was obtained from two sets of 57 nanometer tall channels with 5 μm and 7 μm top wall thickness.

Table 7: Fluid Constants for a Nanoscale Parabolic Cross-Sectioned Channel

	Surface Tension	Dynamic Viscosity	Advancing Contact Angle	Fluid Temperature
	Nm	Pa-s	Degrees	Degrees C
Ge 57 nm – 1 μm top	.0676 ± .002	1.443×10^{-3}	17.5	23

3.2 Nanoscale Channels

In this section the nanoscale channel fabrication process is described, and results are provided for contact angle measurements with sacrificially etched nanochannels. Channel height measurement processes, images, and results are also provided for parabolic nanochannels. Top channel wall thickness was also changed to induce bowing in nanochannels.

3.2.1 Nanoscale Channel Fabrication Process

Standard photolithographic methods were used for fabricating nanochannels. The fabrication of the parabolic channels was carried out in a cleanroom facility. The process began with clean silicon wafers (Fig. 6). A layer of silicon oxide is coated on a silicon wafer to a thickness of over 200 µm via plasma enhanced chemical vapor deposition with a PlasmaLab Model DP800 (Fig. 6A). The top of this wettable layer constitutes the bottom of the channel.

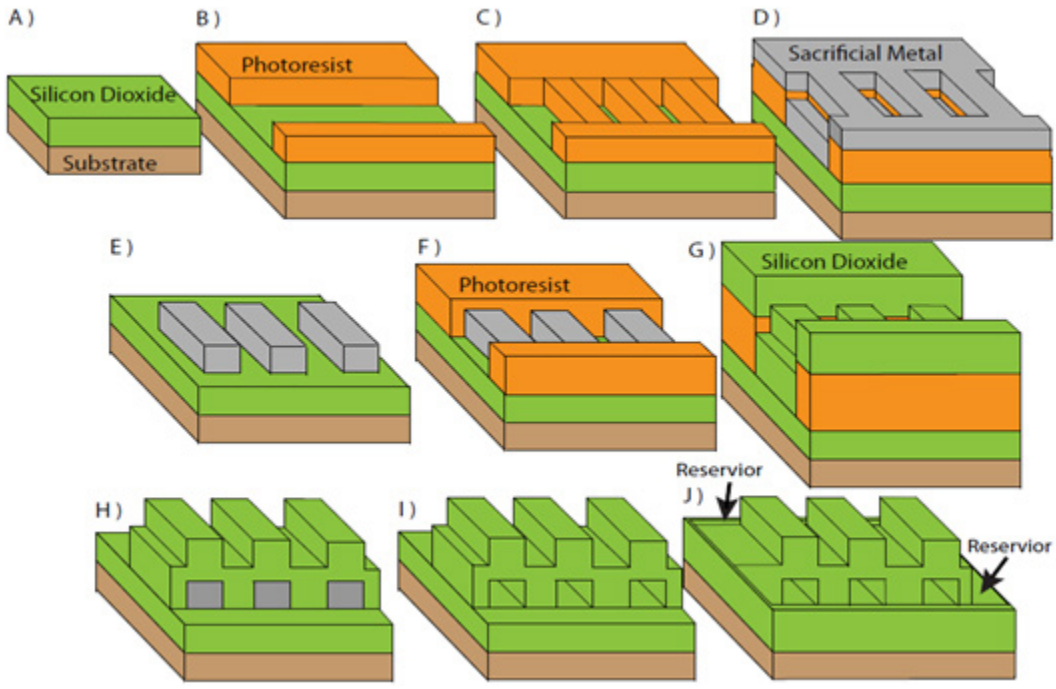

Figure 6: Schematic showing 10 sequential steps necessary to create nanochannels with reservoirs at each channel end.

SU-8 photoresist is spun-on, then the wafers are loaded into a MA150 Karl Suss Aligner to react the photoresist with ultraviolet light (Figures 6B and 6C). This aligner is able to pattern geometry with a half micron tolerance. This photoresist pattern creates the features for the fluid reservoirs and the channel paths. The unreacted photoresist is removed from the wafer using acetone.

A layer of aluminum is then deposited which defines the channel height (Fig. 6D). Aluminum, the sacrificial metal, was substituted with other metals, i.e. chromium and germanium, during the production of other channels. The reacted photoresist is then removed from the silicon wafer (Fig. 6E). The wafers are coated a second time with SU-8 photoresist, to create the channel reservoirs (Fig. 6F). The photoresist is chemically hardened as before, then a top layer of silicon dioxide is coated on top of the entire channel (Fig. 6G). The photoresist is removed to reveal the channel reservoirs, one at each end (Fig. 6H). The sacrificial metal is etched at 50 C^{o} using an aluminum etchant from Transene (Fig. 6I). Chromium cores were etched using commercial strength hydrogen peroxide; however, etch rates were slow, and appeared to produce damaged channel entrances and exits. Germanium cores were used to create parabolic channels as the quick etching rate left the channel entrance and exits undamaged as seen under a microscope. Germanium cores were etched with Transcene 1020 commercial etchant. The formed reservoirs' height was always taller than the nanochannel height (Fig. 6J). Aluminum and germanium cores were soaked with one of four surface treatments, i.e. acetic acid, aqua regia, nanostrip, or sulfuric acid, to finish the sacrificial etching. The channels were rinsed with de-ionized water subsequent to etching. The thickness of the channel's top silicon dioxide layer controls the amount of bending resulting from capillarity. Parabolic channels utilized a thickness of 1 micrometer.

3.2.2 Nanoscale Channel Height Measurement

Nanochannel heights were calculated by the height change in profilometer measurements. First, the silicon dioxide layer was measured via profilometer after the thermal oxide had been applied. Second, the metal was deposited via a thermal evaporator system, and a second profilometer reading was taken. Third, the two profilometer heights were subtracted to obtain a measure of the channel height. Finally, the silicon dioxide top layer was layered on through chemical vapor deposition, and the channel was re-measured to obtain the top wall thickness. Generally, each channel height was known to within 5 nanometers of the nominal height. Specific height values will be presented in Chapter 4.

Nanoscale channel height measurements for a single parabolic channel were taken with a scanning electron microscope as profilometer measurements would dynamically distort the top wall. A 57 nanometer tall channel, obtained by profilometer, with a 1 μm thick top wall was shown to exhibit bowing in the channel's transverse direction for the entire channel length. Germanium cores were etched with Transcene's 1020 commercial etchant in order to minimize entrance degradation. The samples for electron microscope analysis were prepared by sectioning the channel after a single fluid experiment. Each 1.2 millimeter long channel deformed in the transverse direction after a liquid plug was introduced. We did not measure the channel height with an SEM prior to introduction of a liquid plug; however, side wall heights were measured by SEM to be 57 nm. In addition, menisci shapes were only found to distort with 1μm thick top walls. Multiple channel top thicknesses were developed to determine which thickness eliminated bowing of the top wall.

SEM Images were also taken of a side wall with rectangular corners and of another near-center location to help determine the largest height near the center of the channel. It was assumed

that the bowing occurred in a parabolic nature as the corner heights are fixed. A portion of the nanochannel chip was measured via profilometer before de-ionized water was introduced which resulted in a channel height of 57 nm.

3.3 Microscale Channels

This section covers the materials used, the cleaning process, the microchannel creation process, and the microscale channel height measurement process used during experimentation. Acrylic was chosen to create the microscale channels.

3.3.1 Microscale Channel Materials and Cleaning Process

Acrylic plates were utilized to fabricate parallel-plate and tapered cross-section channels. A standardized cleaning process was created to ensure quality channels. Before channel assembly was performed, the acrylic substrates were scrubbed with a Q-tip thoroughly wetted with acetone. The acrylic was then rinsed with deionized water, isopropanol, and again with deionized water. The cleansing process did not affect the static or dynamic contact angles.

All fabrication steps, provided below, were performed in a cleanroom to minimize the amount of dust particles that could adhere to the channels during assembly. Channels were assembled with Double Sided Scotch Tape (3M). The tape uniformly measured 98.5 micrometers thick with a micrometer. To create a tapered channel, one side of the channel was layered with one to two layers of double sided tape. The opposite side of the channel was layered with three to four layers of tape depending on the desired height. The top acrylic layer was then placed on top of the sub-assembly. The final assembly, shown schematically in Fig. 7, was measured again via micrometer, and the original acrylic plate thicknesses were subtracted from the final assembled height to obtain the internal geometry dimensions and determine the channel height.

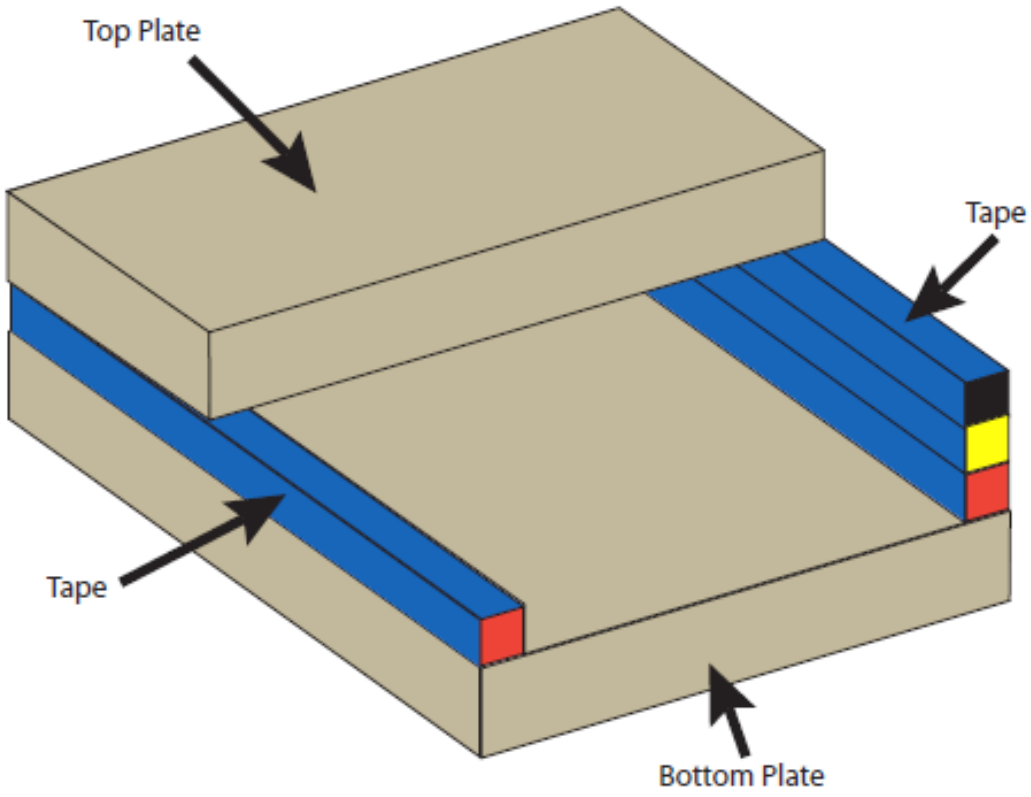

Figure 7: Assembled microscale channel schematic for a tapered cross-section.

Acrylic plates of equal thickness were employed for the walls of linearly varying microchannels. The achieved width to height ratios ranged from 900 for a 98.7 µm tall channel to a ratio of 211 for a 420 µm tall channel. This closely mimics the width to height ratio of 350 for the 57 nm tall nanochannels.

3.3.2 Microscale Height Measurement

The following procedure was used to quantify the height of acrylic microchannels. First, the individual plates were measured with a micrometer to determine the plate thickness. Second, the channel was assembled using the manufacturing process described above. Third, the entire channel thickness was measured. Fourth, the whole thickness was subtracted by the thickness of

each plate to give the channel height across the width of the channel. The Mitutoyo model 293-340, zero to one inch digital micrometer, with a resolution of half of a micrometer was used for all measurements. The channel was measured twenty to forty times along both sides of the channel length each time the channel was assembled. A linear gradient was assumed between the farthest inward measured points.

The acrylic plates were assembled to minimize height variation (Fig. 8). For calculations involving the channel height, the average of the entire channel length was considered, even though the channel height varied by up to 70 micrometers from one end of the channel to the other. The channel height and height variation are plotted according to the furthest inward measureable location (from each side) due to the micrometer physical constraints. The furthest inward measureable location was 28 millimeters from the inside surface of the channel side walls.

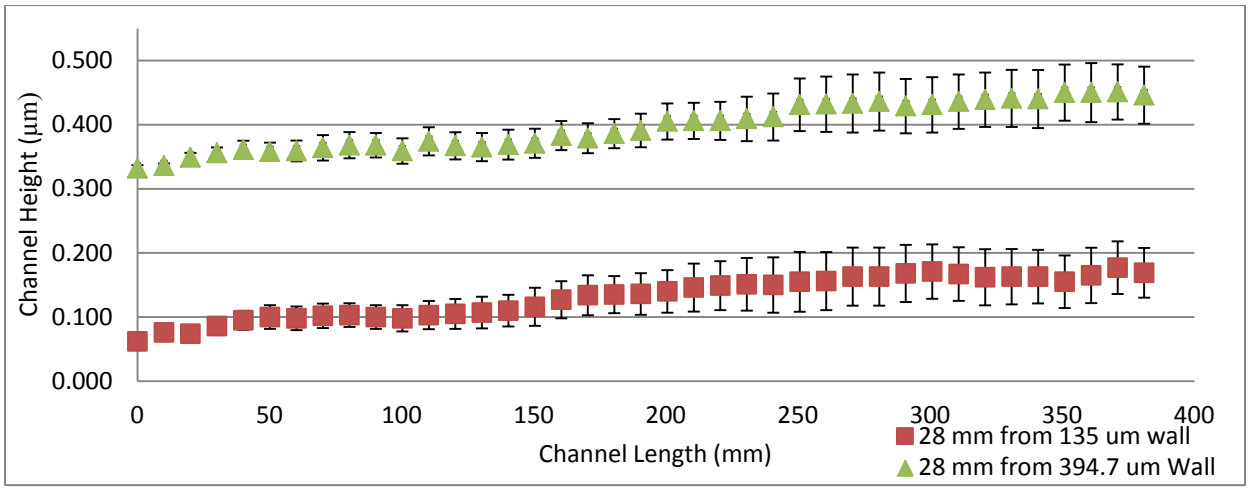

Figure 8: Tapered cross-section heights, measured 28 millimeters from each channel edge, versus length for a 4 inch by 15 inch acrylic channel.

A linear gradient was assumed between the values reported. The channels were permanently marked such that these heights were recreated each time the channels were disassembled, cleaned, and reassembled.

3.3.3 Microscale Channel Apparatus

The apparatus and fluid loading mechanism are explained. The channel was leveled while resting on the apparatus by positioning it on a microscope stage as shown in Figure 9. A mirror was placed at a 45 degree angle to allow the high speed camera to remain horizontal.

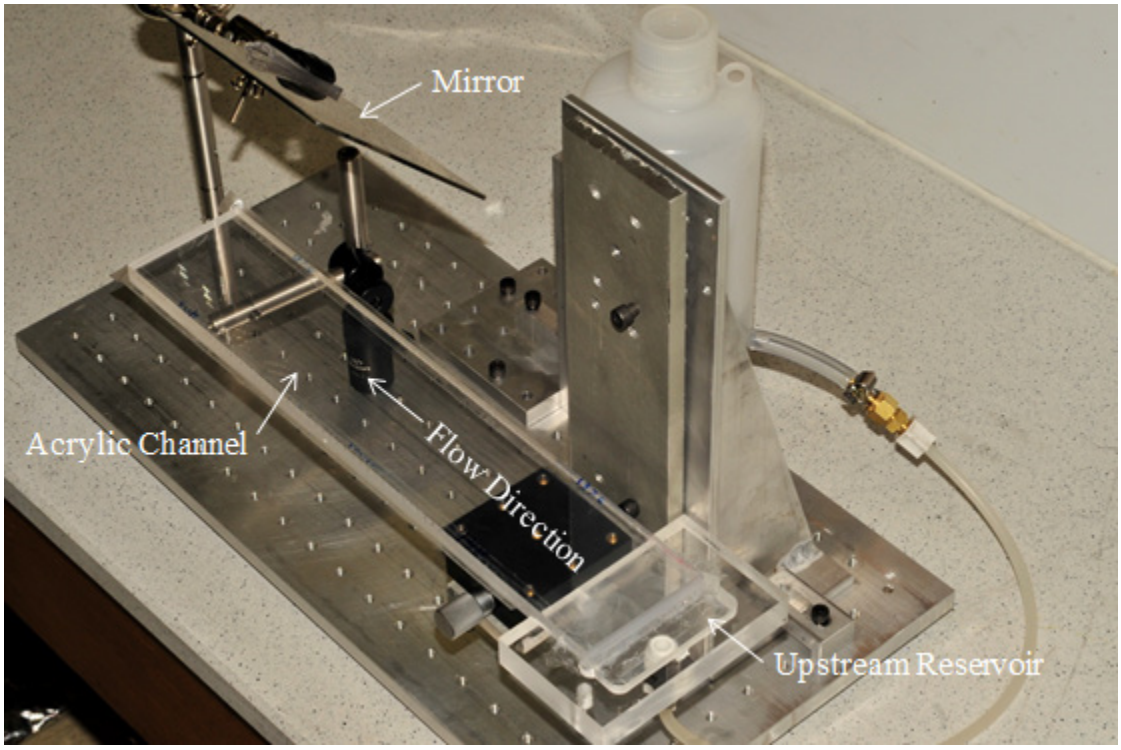

Figure 9: Apparatus for parallel-plate and tapered cross-section experiments

De-ionized water, isopropanol, and methanol were employed for channel filling. In order to eliminate the creation of a pressure head, the reservoir was allowed to spill over if the head reached 1 mm of water over the channel entrance. The flow was recorded using a Photon AP-RX

high speed camera at 60 or 125 frames per second depending on the fluid filling rate thereby capturing the elapsed time. The optical images captured the meniscus as it progressed through the channel.

3.4 Meniscus Tracking Program

A program was created to track the meniscus from the start of each experiment until the high speed camera's two gigabytes of memory was exhausted (approximately $t = 33$ seconds for 60 frames per second) in order to create a plot of the square of the meniscus location as a function of time. This section covers the maximum or minimum seeking function and the sliding slope function used to analyze filling images. Next, the algorithm's application on a microscale channel is discussed. Finally, nanochannels are discussed and how zipper-flow meniscus locations were obtained. Zipper-flow is the flow pattern where the fluid at the channel side walls fills much faster than the center located meniscus.

3.4.1 Maximum or Minimum Algorithm

A maximum or minimum seeking function was employed initially to search for the meniscus location by identifying the highest or lowest value of light intensity within each channel image. A light was externally positioned to illuminate the meniscus interface, increasing the pixel intensity of the meniscus in the image to a value near 255, which is the camera's recordable limit. Background pixel intensities in the image lie near a value of 50. MATLAB's *max* function was used to identify the maximum intensity and location from a given array of pixel values. Therefore, the meniscus location correlated to the maximum pixel intensity value. In low contrast scenarios, Adobe Photoshop was used to darken the entire image, and the

meniscus was brightened to allow the *max* function to correctly find the meniscus without manipulating the meniscus filling data directly.

3.4.2 Sliding Slope Algorithm

The second method for meniscus tracking employed a curve fit function across defined intervals along the channel length. This approach more accurately found the meniscus location. Light intensity for each point in a segment of the channel length was plotted and fit with a line or curve. The slope of each curve fit for each overlapping segment was determined. Maximum slope values occured before the meniscus due to the large change from dark to light pixel intensity values. This method used a sliding slope polynomial fitting function known as *polyfit* in MATLAB. The *max* function obtained the location of the meniscus interface corresponding to the largest slope. The process was repeated across the channel width for each image taken during the experiment.

At the channel level, the maximum intensity locations across the channel were stored for each image frame to re-create the meniscus location. Three areas were tracked for channels exhibiting zipper flow. The pixel locations near the side walls were tracked and averaged as they exhibited the same channel height. The parabolic channel center was then tracked via either of the above described methods.

4 RESULTS AND DISCUSSION

Results of filling experiments for microscale and nanoscale channels are compared to theoretical predictions from the classical and modified Washburn equations. The outcomes for microscale parallel-plate acrylic channels are discussed first. Next, results for microscale tapered acrylic channels are presented, and the use of an effective channel height is evaluated as a prediction method. Subsequently, nanoscale parallel-plate channel results are presented for various channel heights, with differing surface treatments, and for different sacrificial metals. Lastly, nanoscale parabolic channel filling results are provided.

4.1 Microscale Acrylic Parallel-Plate Channels Results

Microscale parallel-plate channel filling experiments were performed with methanol, isopropanol, and deionized water in order to calculate the advancing contact angle. The meniscus advancement for methanol and isopropanol was essentially uniform and perpendicular to the entrance plane for all flow sets. Deionized water had a meniscus front of non-uniform shape for all microscale channel filling experiments, which is evidence of a changing advancing contact angle across the channel cross-section. The square of the meniscus position in the channel was graphed as a linear function of time, and the slope was compared to the theoretical Washburn values. The fluids are considered individually in the following sections. The advancing contact

angles were computed for each fluid from the experimental L^2 versus t data for each data set and are summarized in section 4.1.4.

4.1.1 Methanol – Acrylic Parallel-Plate Microscale Channel

The advancement of methanol was tracked through a channel segment with a height of 186 ± 15 µm. The large uncertainty in the channel height is due to the acrylic plate deviation over the length of the captured experimental flow where the channel entrance measured 171 µm. The filled length of channel measured 7.75 inches long with a height of 201 µm. Over the entire 15 inch long channel, the height was approximately 70 µm greater at the channel exit than at the entrance (see Figure 8). Figure 10 shows the square of the meniscus position, L^2, versus time for methanol in the parallel-plate channel. A linear regression analysis of the L^2 versus time data provided a slope of 3687.3 mm^2/s.

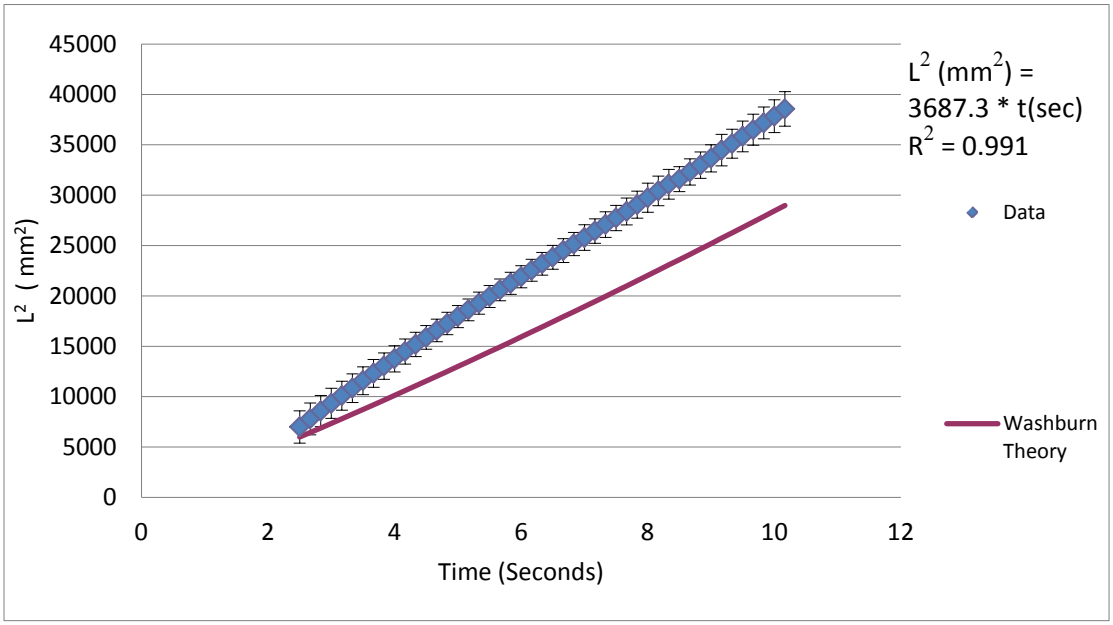

Figure 10: Square of the meniscus location vs. time for an acrylic parallel-plate channel with the wall-to-wall spacing of 186 um and with methanol as the working fluid. The error bars correspond to a 95 percent confidence interval of the mean for n=3.

The error bars in Figure 10 correspond to a 95 percent confidence interval of the mean for the three repeat experiments. The meniscus shape and the advancing contact angle were uniform for all flow sets as can be deduced from the linear slope of the advancement of the meniscus front as explained in section 3.1.2. The advancing contact angle was found to be zero as the inverse cosine cannot be taken for values greater than one. The plotted Washburn theory line in Figure 10 utilizes the advancing contact angle and the varying height at each location in the microscale channel. The experimental data exceeds, on average, the predicted behavior based on the Washburn theory by 36 percent. The large deviation from the Washburn equation suggests an error in the dynamic viscosity, as all other constants have been experimentally measured.

4.1.2 Isopropanol – Acrylic Parallel-Plate Microscale Channel

The second fluid of interest, isopropanol, was tracked through a 223.5 ± 14.5 µm tall section of a parallel-plate channel over a filling length of 6.6 inches. The slope of the isopropanol L^2 versus time from the regression analysis was 972.2 mm^2/s (Figure 11).

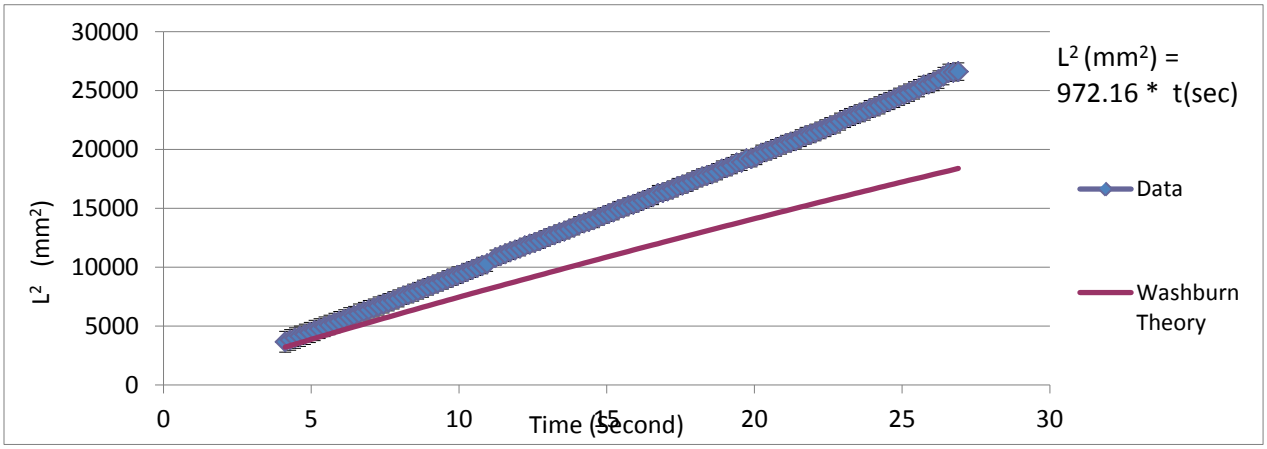

Figure 11: Square of the meniscus location vs. time for an acrylic parallel-plate channel with the wall-to-wall spacing of 233 um and with isopropanol as the working fluid. The error bars represent the 95 percent confidence interval of the mean for n=3.

The meniscus shape and the advancing contact angle were uniform for all flow sets, and the advancing contact angle was found to be zero. The experimental capillary flow of isopropanol surpasses the classical Washburn theory by 32 percent on average when using the advancing contact angle in the calculations. Again, the large deviation from the Washburn equation suggests an error in the dynamic viscosity.

4.1.3 Deionized Water – Acrylic Parallel-Plate Microscale Channel

The experimental flow data for deionized water was acquired using an acrylic channel with a height of 293.5 ± 11.5 μm over a filling length of 6.6 inches. The deionized water experiments resulted in flow patterns with unexpected meniscus shapes. The data displayed in Figure 12 is from a single experiment due to large changes and variability in contact angle; however, repeated experimentation resulted in similar results. While a parallel-plate channel should produce a straight meniscus, the experimental result showed otherwise. A changing advancing contact angle may account for the non-straight meniscus shape; dynamic viscosity or a channel height deviation across the width of the channel would result in an overall angular shift in the meniscus front. Figure 12 reports the square of the meniscus position versus time, and the data deviates from the Washburn theory (adjusted for channel height) by an average of 4.9%. A higher frame rate (250 frames per second) was used to increase confidence in the observed meniscus shape and position data.

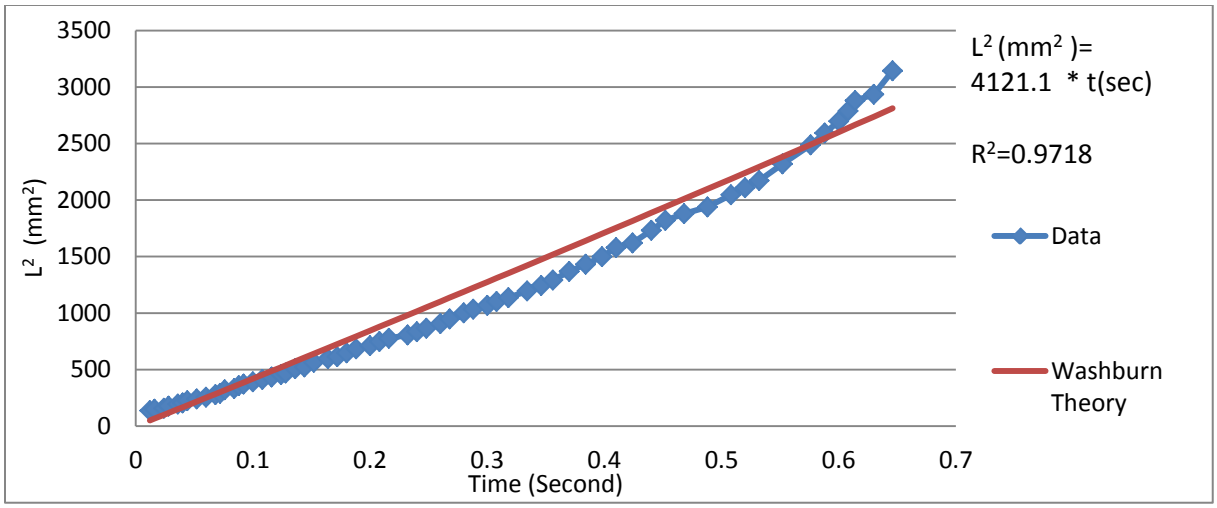

Figure 12: Square of the meniscus location vs. time for an acrylic parallel-plate channel with the wall-to-wall spacing of 156.5 um and with deionized water as the working fluid.

The deionized water filling data had a linear slope of 4121.1 mm^2/s. The resultant advancing contact angle was found to be 28 degrees. The calculated constants and values are summarized in section 4.1.4.

4.1.4 Acrylic Parallel-Plate Summary

Averaged experimental data for the filling of acrylic parallel-plate microscale channels with methanol, isopropanol, and water were used to calculate each fluid's advancing contact angle using the Washburn equation (Eq. 1) solved for θ_{adv} (Table 8). The value of the inverse cosine of the advancing contact angle for methanol and isopropanol was greater than one, so the advancing contact angle was assumed to be zero (equivalent to the static contact angle). The data sets for each fluid were then compared to the Washburn equation calculated with their respective experimentally determined advancing contact angle. The difference between the experimental and theoretical L^2 versus time values was approximately 30% for methanol and isopropanol. This could be due to the variation in channel height over the length of the channel or a difference between the actual and tabulated values for dynamic viscosity. The calculated

advancing contact angles for methanol, isopropanol, and water from these parallel-plate experiments were applied in the following section to predict flow in non-parallel plate microscale channels using the modified Washburn equation.

Table 8: Calculated Advancing Contact Angle Constants for Acrylic Parallel-Plate Channels

	Static Contact Angle θ	Experimental L^2/t	Experimental $\cos(\theta_{adv})$	Advancing Contact Angle θ_{adv}	Difference of Experimental L^2/t from Classical Washburn Theory using θ_{adv}
	Degrees	m^2/s	None	Degrees	Percent
Methanol	0	3687.3	1.41	0	34.3
Isopropanol	0	972.2	1.33	0	32.2
Deionized Water	65.2	4121.1	0.88	28.1	-4.9

4.2 **Microscale Acrylic Tapered Channels**

The following sections provide filling data for non-parallel plate microscale channels with three different fluids. The acrylic channels were assembled with tapered cross sections. The filling data for tapered channels revealed large increases in filling speeds for smaller channel heights and large decreases in filling speeds for the taller channel heights, which is opposite to the expected parallel-plate slope values. This trend is correctly predicted by the modified Washburn equation in conjunction with Eq. 15 from Chapter 2. Filling results show that the meniscus at the taller channel height trailed behind the meniscus at the shorter channel height, as expected. The effective height/slope correlation for tapered channels from the modified Washburn equation deviated from theory by 10.1 and 3.33 percent for methanol and isopropanol, respectively. Deionized water experimental results showed larger run to run variation than

methanol or isopropanol due to a changing advancing contact angle and had a deviation of 14.7 percent from the modified Washburn theory. The following sections are organized by fluid of interest.

4.2.1 Methanol – Tapered Microscale Channel

Fluid advancement was tracked in an acrylic channel with a tapered cross section with channel heights measuring 381.55 µm on the tall side to 148.45 µm on the short side of the taper. An effective height of 219.65 µm was calculated from the model developed previously in Chapter 2. The meniscus filling data for the tallest channel height matches the modified Washburn equation utilizing the effective height in Figure 13.

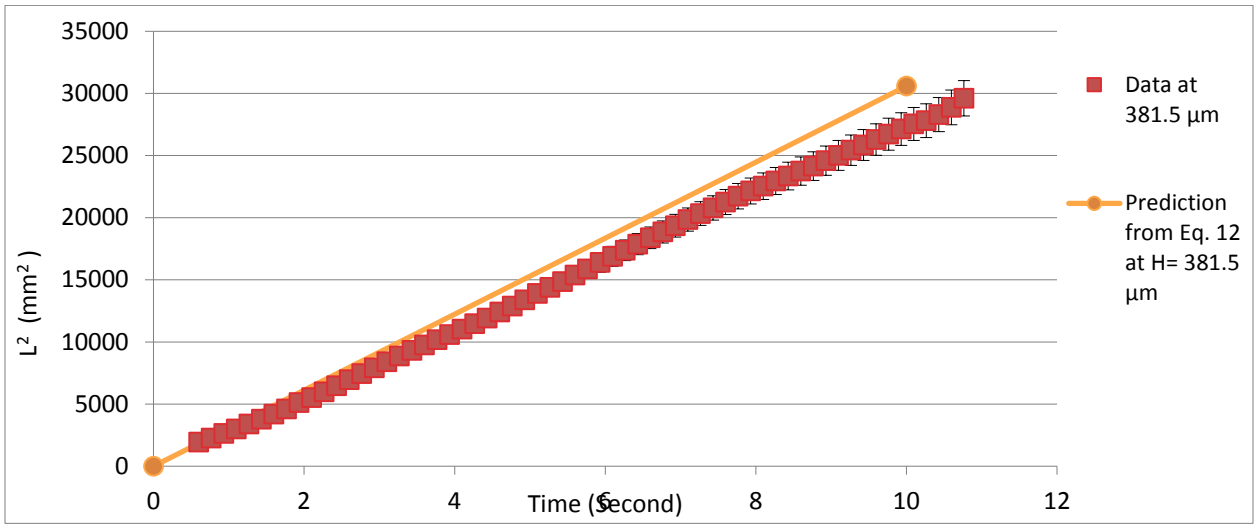

Figure 13: Square of the meniscus location vs. time for an acrylic channel exhibiting a tapered cross-section with the wall-to-wall spacing of 381 µm.

Using linear regression analysis, a slope of 2749.1 mm^2/s was obtained for the tallest experimental height. Comparing the modified Washburn equation value to the experimental data shows an error of only 10.1 percent while using an advancing contact angle of zero and a

dynamic viscosity that was linearly interpolated from an average temperature of 23.5 ºC. The modified Washburn equation correctly assumed that the effective height characterizes the pressure gradient created by the varying wall-to-wall cross-sectional spacing. As explained in Chapter 2, the largest slope (L^2 vs. t) correlates with the smallest channel height and not the tallest channel height, which agrees with experimental observation. The effective channel height correlation more accurately predicted the square of the methanol meniscus position as a function of time than the classical Washburn equation.

Table 9 provides a summary of the calculated values for Figure 13 where the channel's effective height of 219 μm provides a closer prediction of the channel's filling data.

Table 9: Methanol – Tapered Microchannel Uncertainty Error

Height	Modified Washburn Theory Slope L_{eff}^2	Linear Regression Experimental Slope	Nominal Deviation from Theory
μm	mm^2/second	mm^2/second	Percent
381.0	3058.4 ± 110	2749.1 ± 12.9	10.1

The remaining channel height data (148.45 and 265 μm) was compared to calculated results from Eq. 15, which predicts the location of the meniscus based on the ratio of the channel's heights and the distance from the channel entrance. The L^2 data was curve fit to reduce noise and obtain S, the difference between filling data between the tallest channel height, 381 μm, and the shortest height, 148 μm. The same approach was applied at the average channel height. A linear regression analysis was performed on the differenced experimental data, S, and on the predicted slope for S at each individual channel height from Eq. 15. The slope values were compared to obtain correctional factors for each height. Figure 14 shows the experimental data compared to

the prediction data with correctional coefficient of 0.32 for S which is the average of the isopropanol and methanol tapered experimentation. In an effort to characterize the three dimensional flow we chose to apply the correctional coefficient, C, to Eq. 15 which results in Eq. 22 where C is an experimentally determined value of 0.32.

$$\boldsymbol{S = CL\left(\frac{H_B}{H(z)} - 1\right)} \qquad \textbf{(22)}$$

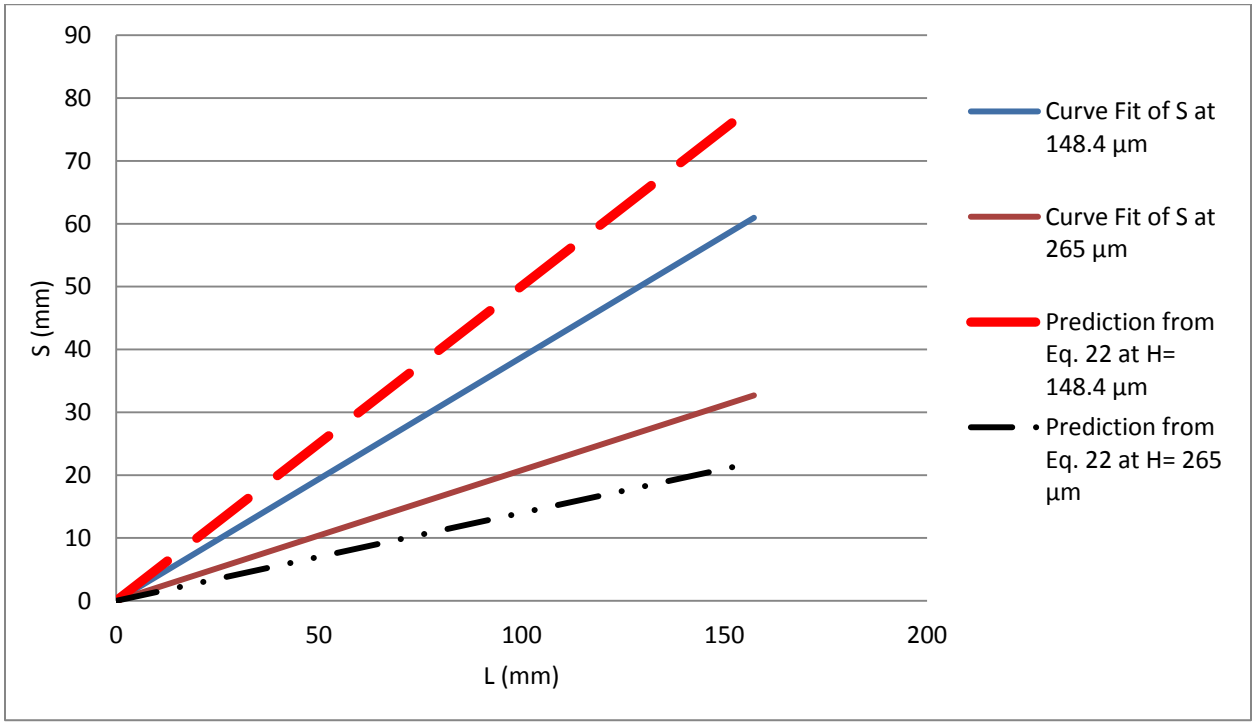

Figure 14: Predicted meniscus locations are compared to methanol meniscus locations for a tapered channel where 381.5 um was determined to be the tallest height.

The data shows that at an increasing distance from the channel entrance, the meniscus will distort more and travel farther the lower the channel height within a channel of constant cross sectional shape. After the correctional coefficient, C, was introduced, Eq. 22 predicts the meniscus distortion location at H = 148 µm to within 23.0% of the experimental data. At H = 265 µm, the prediction is within 48.5% of the experimental curve fit.

4.2.2 Isopropanol – Tapered Microscale Channel

Isopropanol channel filling experiments followed the same general behavior as the methanol. Using an effective channel height of 219.65 µm, an advancing contact angle of zero degrees, and a dynamic viscosity linearly interpolated for an average temperature of 23 ºC, the modified Washburn equation was calculated from the experimental model developed previously. Figure 15 provides the isopropanol experimental data for a tapered channel exhibiting a height variation from 381.5 µm to 148.4 µm, where data shown at a channel height of 148 µm correspond to the location of the tracked meniscus front at the small side of the tapered channel. Data at 265 µm is the center plane between the tall and short sides of the tapered channels.

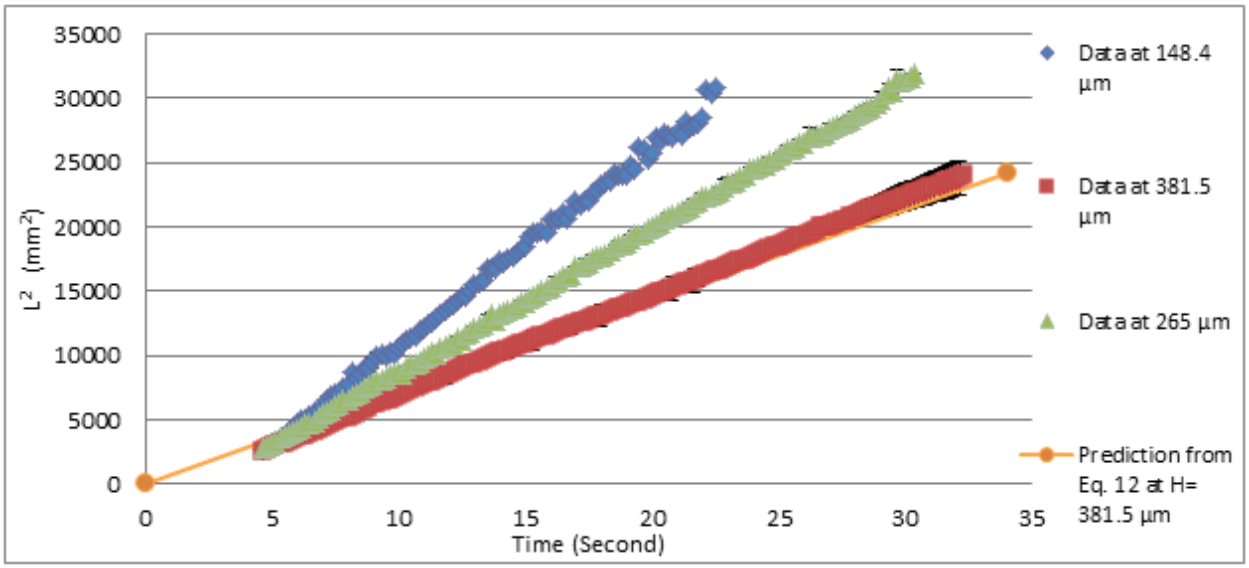

Figure 15: Square of the meniscus location vs. time for an acrylic channel exhibiting a tapered cross-section with the wall-to-wall spacing of 381.5 µm to 148.4 µm and with isopropanol as the working fluid.

The modified Washburn theory and the experimental filling L^2/t values for the tall channel height contained in Table 10 were in excellent agreement, with the resulting difference between the linear regression for the tallest channel height and the modified Washburn equation of only 3.33 percent.

Table 10: Isopropanol - Tapered Microchannel Uncertainty Error

Height	Modified Washburn Theory Slope L_{eff}^2	Linear Regression Experimental Slope	Nominal Deviation from Theory
µm	mm^2/second	mm^2/second	Percent
381.5	711.7 ± 22.3	735.4 ± 13	3.33

The data for the medium and small channel heights were compared to results from Eq. 22, which predicts the location of the meniscus based on the ratio of the channel's heights and the distance from the channel entrance including the correctional coefficient *C*. Figure 16 shows the data with a correctional coefficient, *C*, of 0.32 in an effort to characterize the three dimensional flow.

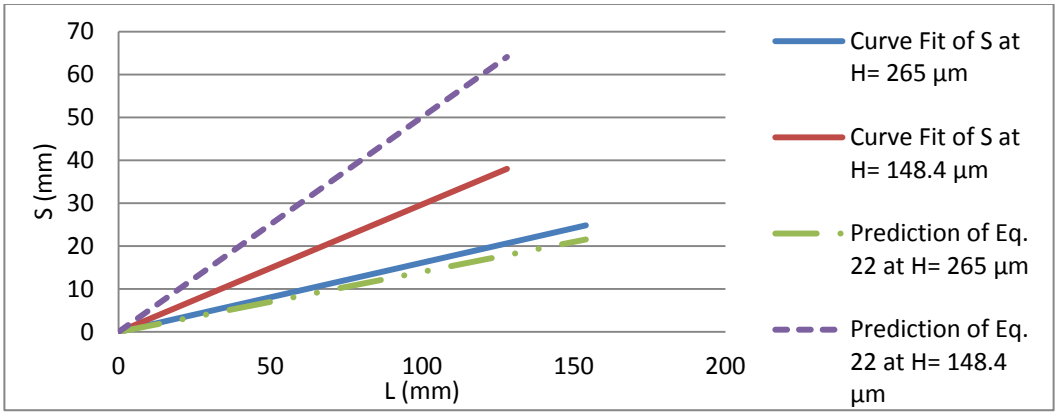

Figure 16: Predicted meniscus locations are compared to actual isopropanol meniscus locations for a tapered channel where 381.5 µm was determined to be the tallest height.

After the correctional coefficient, *C*, was introduced, Eq. 22 predicts the meniscus distortion location at H = 148 µm to within 68.6% of the experimental data. At H = 265 µm, the prediction is within 13.2% of the experimental curve fit.

4.2.3 Deionized Water – Tapered Microscale Channel

A complicated flow pattern was observed for tapered microscale channels filled with deionized water. The square of the meniscus location versus time for deionized water in a tapered channel exhibiting a height of 381.5 µm to 148.4 µm can be seen in Figure 17. Due to the erratic nature of the meniscus, which can be explained by an actively changing advancing contact angle, the slope for the tall channel height was similar to the slope for the shorter channel height and changed down the length of the channel. The values for the modified Washburn equation were calculated from the experimental model developed in this study using an effective height of 219 µm and an advancing contact angle of 28.1 degrees based on the parallel-plate experiments (Section 4.1.3). The dynamic viscosity was linearly interpolated to an average temperature of 24 ºC. The 95 percent confidence levels were not plotted as the error bars overlapped making it difficult to view each separate confidence interval.

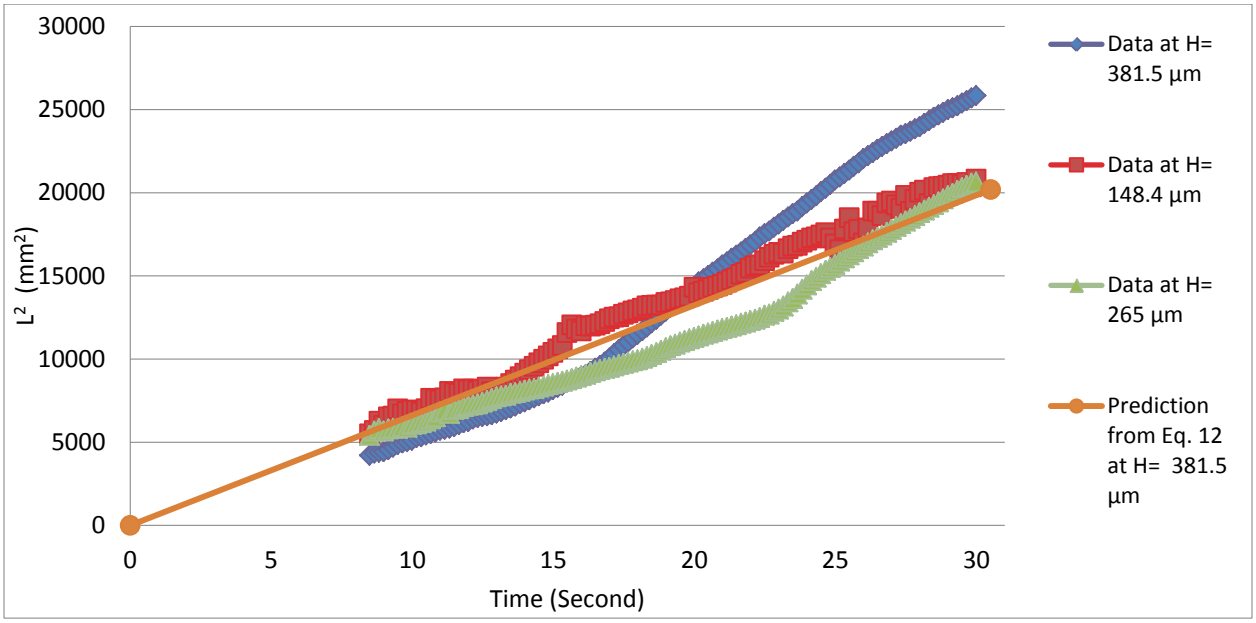

Figure 17: Square of the meniscus location vs. time for an acrylic channel exhibiting a tapered cross-section with the wall-to-wall spacing of 381.5 µm to 148.4 µm and with deionized water as the working fluid.

Table 11 provides a summary of the calculated values for Figure 17 and the uncertainty error as the tolerance band for the theoretical and experimental filling rates. The tapered filling slope of deionized water based on the parallel-plate advancing contact angle led to a deviation greater than 50%. The advancing contact angle was solved for a second time for each channel height section. The contact angles found were much higher than previously noted. The Washburn theory line produced is shown with the re-calculated advancing contact angle based on the flow data used to create Figure 17.

Table 11: Deionized Water - Tapered Microchannel Uncertainty Error

Height	Modified Washburn Theory Slope L_{eff}^2	Linear Regression Experimental Slope	Deviation from Theory
µm	mm^2/second	mm^2/second	Percent
381.5	662.0 ± 118.3	759.7 ± 12.9	14.7

As the experiment was performed three times with similar results, the change in contact angle may have occurred based on channel cleanliness. The erratic meniscus front behavior was likely due to a radically changing contact angle. The meniscus front for all microscale channel experiments with deionized water was non-perpendicular and highly deviant to the channel entrance as can also be seen by the large confidence intervals. Deionized water presented the same issue for both acrylic substrates and glass substrates. Tapered and parallel-plate channels were rebuilt numerous times in order to deduce if an external factor was being introduced; however, none was found. Therefore, it was deemed appropriate to recalculate the advancing contact angle for deionized water.

The remaining channel height data could not be compared to Eq. 15 which predicts the location of the meniscus based on the ratio of the channel's heights and the distance from the channel entrance due to a changing advancing contact angle throughout the deionized water experiment. Eq. 15 assumes the advancing contact angle is constant, whereas the deionized water experimentation manifested a non-uniform meniscus front and dynamic advancing contact angle.

4.3 **Nanochannel Parallel-Plate Channels**

Aluminum, chromium, and germanium parallel-plate channel filling results which were used to calculate the advancing contact angle for different channel heights and surface treatments are presented. All channels, except for the 57 nm germanium channel height, were created with a top wall thickness greater than 3 μm to prevent channel bowing. The square of the meniscus location as a function of time were compared to theoretical values for each channel height and chemical surface treatment. The advancing contact angles were also calculated for each set of data. Figure 18 is a photograph of a single nanochannel chip representative of all nanochannels presented in this study. The filling reservoir is located on the left hand side, water flows through each 20 μm wide channel until the channel exit, shown on the right hand side.

The dark region on the left of Figure 18 was water overspill from the reservoir. The meniscus tracking program was set to disregard this data entirely by limiting the searchable field to the area located to the right of the overspill area. The channels were spaced 20 μm apart with a nanochannel flow width of 20 μm for each channel.

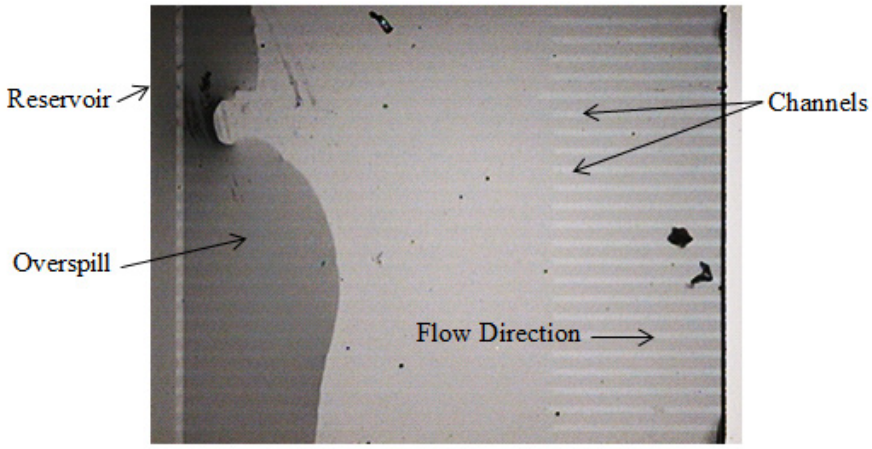

Figure 18: 19.5 nm aluminum etched parallel-plate nanochannel chip

Channels of 57 nm height and fabricated with germanium as the sacrificial metal had channel top thicknesses that were modified to study the effects of channel bowing. The channel tops were deposited with the following thicknesses: 1 µm, 3 µm, 5 µm, and 7 µm. These thicknesses were used to study L^2/t as a function of channel top thickness. Channels with 1 µm exhibited parabolic bowing as was evident during data collection and scanning election microscope photographs. The advancing contact angle calculated from germanium etched 57 nm parallel-plates with a 7 µm top thickness were used in the 1 µm thick top parabolic channel modified Washburn analysis.

4.3.1 Aluminum Core Sacrificially Etched Channels

Aluminum sacrificial core parallel-plate nanochannels were created to study the square of the meniscus versus time, L^2/t, for nanoscale channels with heights of 19.5 ± .5 nm, 55 ± .5 nm, and 88.5 ± .5 nm. Table 12 provides the summarized results for each of the aluminum core etched channels. The advancing contact angles were calculated from the parallel-plate channels of different heights as follows. Linear regressions were performed for each averaged data set to

determine the experimental slope (L^2/t) and this was used to calculate the advancing contact angle using Equation 21 in Section 3.1.2. The Washburn theoretical slope (L^2/t) values are reported along with the experimental slope values.

Table 12: Aluminum Summary – Nanochannel Slopes with Uncertainty Values

Material Height – Surface Treatment	Washburn Theory L^2/t Slope	Experimental L^2/t Slope	Advancing Contact Angle θ_{adv}
Nanometer	mm^2/second	mm^2/second	Degrees
Al 19.5 - Acetic Acid	0.057 ± .027	Collapsed	Collapsed
Al 19.5 - Aqua Regia	0.057 ± .027	0.054 ± .003	79.8
Al 19.5 - Nanostrip	0.057 ± .028	0.534 ± .003	79.9
Al 19.5 - Sulfuric Acid	0.057 ± .028	0.064 ± .003	77.8
Al 55 - Acetic Acid	0.468 ± .125	0.473 ± .010	56.6
Al 55 - Aqua Regia	0.468 ± .125	0.466 ± .010	57.1
Al 55 - Nanostrip	0.468 ± .132	0.478 ± .010	56.2
Al 55 - Sulfuric Acid	0.468 ± .132	0.455 ± .010	58.1
Al 88.5 - Acetic Acid	1.015 ± .193	1.071 ± .003	39.2
Al 88.5 - Aqua Regia	1.015 ± .193	0.916 ± .003	48.5
Al 88.5 - Nanostrip	1.015 ± .204	1.094 ± .003	37.7
Al 88.5 - Sulfuric Acid	1.015 ± .204	0.978 ± .003	45.0

In all cases the advancing contact angle increased from the corresponding static contact angle for each decreasing channel height. All experiments resulted in feasible arccosine calculations. Therefore, it appears that the advancing contact angle is highly dependent upon

channel height and decreases with channel height. The Washburn theory uncertainty value was high due to the variation of the meniscus locating algorithm (± 4 pixels of the actual location). Dynamic viscosity uncertainty was the second largest contributor to the Washburn theory uncertainty values.

4.3.2 Chromium Core Sacrificially Etched Channels

A summary of chromium core parallel-plate nanochannels and their respective square of the meniscus location as a function of time are given in Table 13. This data was used to calculate the advancing contact angle for parallel-plate channels. Channel heights of 71.5 ± .5 nm and 86.5 ± .5 nm were created from chromium and table 13 provides the summarized results for all chromium etched channels.

Table 13: Chromium Summary - Nanochannel Slopes with Uncertainty Values

Material Height – Surface Treatment	Washburn Theory L^2/t Slope	Experimental L^2/t Slope	Advancing Contact Angle θ_{adv}
Nanometers	mm^2/second	mm^2/second	Degrees
Cr 71.5 - Nanostrip	0.887 ± .125	0.887 ± .003	37.4
Cr 86.5 - Acetic Acid	1.21 ± .192	1.225 ± .003	24.9
Cr 86.5 - Aqua Regia	1.21 ± .192	1.289 ± .003	17.4
Cr 86.5 - Nanostrip	1.21 ± .148	1.084 ± .003	36.6
Cr 86.5 - Sulfuric Acid	1.21 ± .192	1.240 ± .003	23.4

In all cases the advancing contact angle was greater than the experimentally measured static contact angles and increased with decreasing channel height, similar to the aluminum cored channels. Each experimental slope (L^2/t) reported was obtained through a linear regression of the data at each height and surface treatement combination. The tolerance values were calculated for

the theoretical filling rate by using the uncertainty of each experimentally measured variable in the Washburn equation to produce the uncertainty band shown.

4.3.3 Germanium Sacrificially Etched Channels

Channels with different top thicknesses of 7, 5, or 3 μm and a constant germanium sacrificial metal height of 57 nm were used to further investigate the effects of deformation on capillary filling speeds and the meniscus curvature. The first set of channels had tops measured to be 7 μm thick. The thick channel top does not allow displacement in the channel walls created from the negative pressure encountered during capillary flow. In addition, the channel tops did not deflect when being measured with a profilometer. The transient flow L^2/t values for the 7 μm thick channel top can be taken as a baseline channel. Similar results were observed for channels with 5 μm thick tops.

The next set of channels was created from a germanium sacrificial metal height of 57 nm with a channel top thickness of 3 μm, which allows approximately 4.2 nm of deflection according to a finite element analysis obtained from Pro Mechanica. The 3 μm thick top filling experiments produced curved menisci; however, the corner meniscus location was not plotted for the data shown. Therefore, we successfully created bowing nanoscale channels in order to show why the classical Washburn predicted behavior has large deviations to experimental data. Figure 19 reports the transient flow L^2/t values in channels with 3 μm thick tops that were slightly lower than channels with 5 and 7 μm thick tops due the deflection in the center of the channel. The resulting deviation between filling rates resulted from channel height bowing.

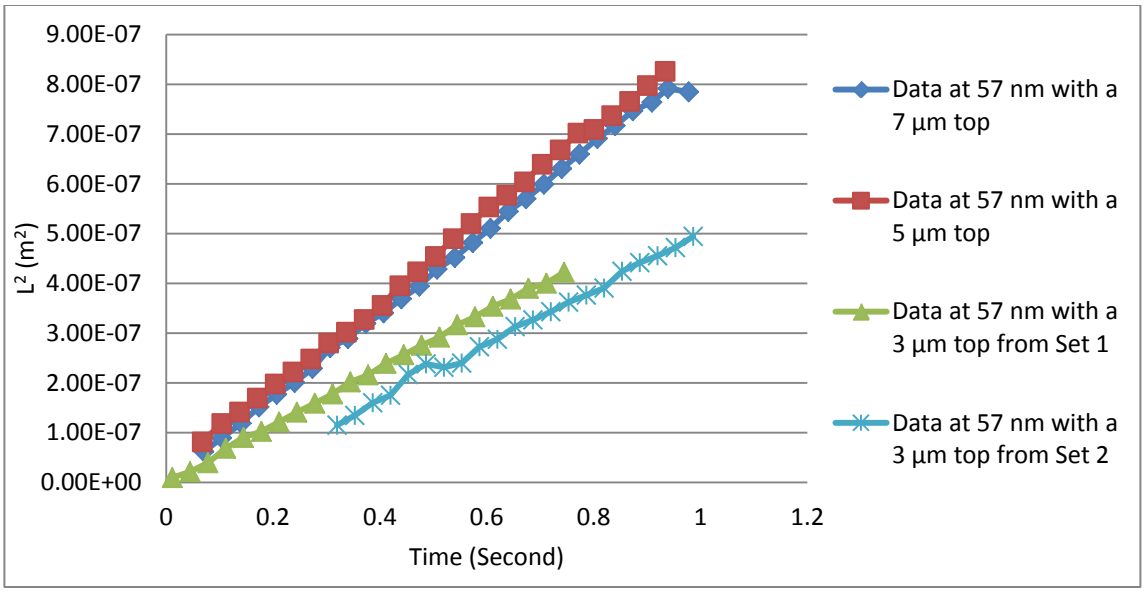

Figure 19: Square of the meniscus location vs. time for glass channels exhibiting a parallel-plate cross-section etched from germanium with 7 µm and 5 µm top wall thickness with wall-to-wall spacing of 57 nm and with deionized water as the working fluid. The 3 µm top wall thick channel exhibits a parabolic cross-section.

The channel top thickness, if not sufficiently thick, can affect the experimental filling data as was seen in the difference between the results for the channels with 3 µm and 7 µm thick tops. The larger the negative pressure experienced in the channels, the larger the channel top wall will need to be to limit deflection.

Channels of 5 and 7 micrometer thick top walls produced a flat meniscus geometry, whereas experimentation with 3 micrometer thick channel tops were significantly different due to bowing, as evidenced by a zipper-like meniscus within the fluid flow. A large deviation in advancing contact angle is another indication of bowing. Each data set is plotted in Figure 20 with an advancing contact angle of 17.5 degrees as measured from the average of 5 µm and 7 µm thick top channel sets. If bowing is neglected, then given a 3 µm thick top, the advancing contact angle would be 53.7 degrees which, measured in terms of the cosine value, is a difference of 37.9%. Figure 20 reports the L^2/t data for germanium etched 57 nm channels with 7 µm, 5 µm, and 3 µm channel top walls.

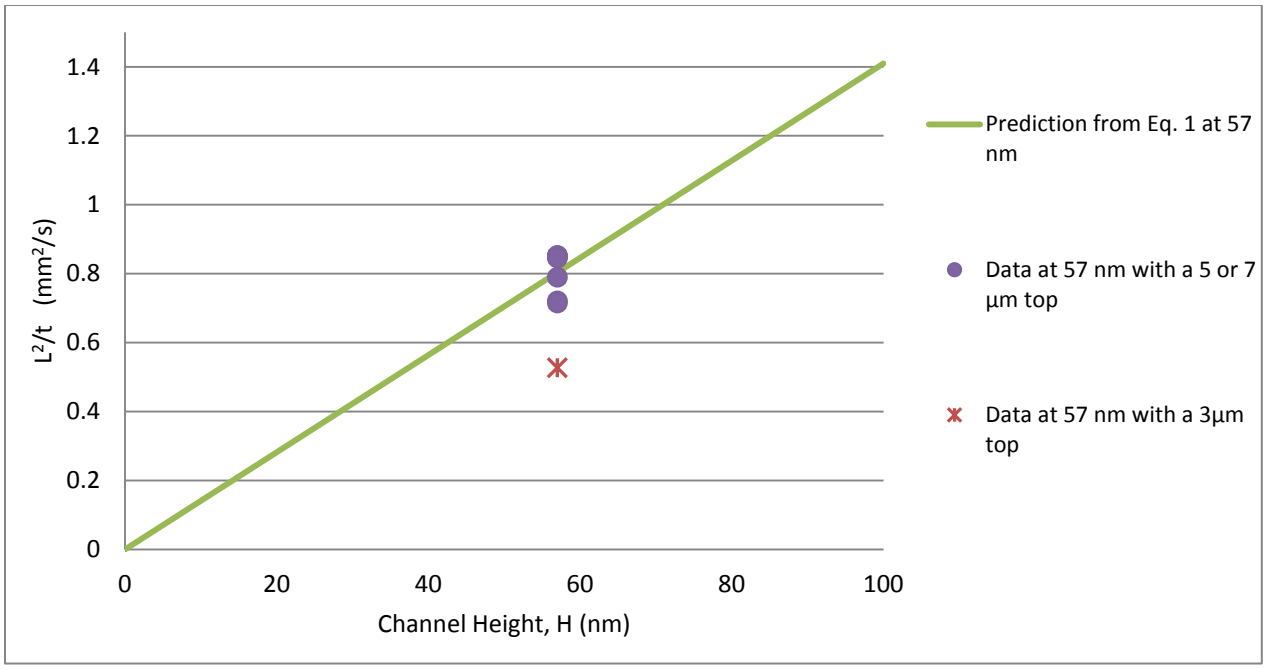

Figure 20: Meniscus experimental slope (L^2/t) vs. channel height for glass channels exhibiting a parallel-plate cross-section etched from germanium sacrificial cores with wall-to-wall spacing of 57 nm and with deionized water as the working fluid.

The classical Washburn prediction from Equation 1 was plotted against the 57 nm experimental data with varying channel top thicknesses. Assuming the advancing contact angle remains the same for each experiment, the 3 µm thick channel top experiments result in a 37.9% deviation from the predicted behavior.

Filling data results obtained through experimentation with germanium etched channels are provided in Table 14. As with the aluminum and chromium advancing contact angles, the germanium contact angles also increased from their experimentally measured static contact angles. Varying surface treatments did not adjust L^2/t significantly, as the values obtained were similar in magnitude.

Table 14: Germanium Summary – Nanochannel Slopes with Uncertainty Values

Material Height – Surface Treatment	Washburn Theory L^2/t Slope	Experimental L^2/t Slope	Advancing Contact Angle θ_{adv}
Nanometer	mm^2/second	mm^2/second	Degrees
Ge 57 - Acetic Acid	0.803 ± .142	0.721 ± .003	35.9
Ge 57 - Aqua Regia	0.803 ±.142	0.790 ± .003	27.5
Ge 57 - Nanostrip	0.803 ± .149	0.852 ± .003	16.9
Ge 57 - Sulfuric Acid	0.803 ± .149	0.849 ± .003	17.6
Ge 57 - Hydrogen Peroxide	0.803 ± .144	0.715 ± .003	36.6
Ge 57 - 3 μm top	0.803 ± .144	0.527 ± .003	53.7
Ge 57 - 5 μm top	0.803 ± .144	0.853 ± .003	16.7
Ge 57 - 7 μm top	0.803 ± .144	0.846 ± .003	18.2
Ge 85.5 - Acetic Acid	0.976 ± .142	0.939 ± .010	45.3
Ge 85.5 - Aqua Regia	0.976 ± .142	1.170 ± .010	28.8
Ge 85.5 - Nanostrip	0.976 ± .149	0.885 ± .010	48.5
Ge 85.5 - Sulfuric Acid	0.976 ± .149	0.910 ± .010	47.1

The Washburn theory slope indicated in the first column was computed from Eq. 1. The experimental slope was obtained via a linear regression analysis which was used to calculate the advancing contact angle for each parallel–plate channel experiment. The advancing contact angle corresponding to the 57 nm channel height with sufficient top wall thickness were employed in the parabolic channel analysis.

4.4 **Nanochannel Parabolic Channels**

The modified Washburn equation correctly predicted the resultant deviation from parallel-plate predicted behavior in tapered microscale channels. In conjunction with adequately describing the minor bowing observed during the filling of channels with a top thickness of 3 μm, it was hypothesized that flow through channels with an even thinner top wall, i.e. 1 μm, could also be predicted with the model. Channels with a height of 57 nanometers and a 1 μm top

thickness were prepared from germanium and tested. Although each channel was initially created with a parallel-plate geometry, the channels deformed upon introduction of the liquid plug, resulting in a parabolic geometry and non-standard fluid flow.

Filling channels with a top less than 3 μm thick produced a deformed meniscus with fluid flow at the channel edges advancing well beyond the meniscus location at the channel's center due to top wall deflection (Fig. 21). Similar results were also observed in aluminum core etched 71 nm tall channels with thin top wall thicknesses. In order to determine the extent of channel deflection, a scanning electron microscope was utilized to quantify the channel height at the corners and near the center of the channel.

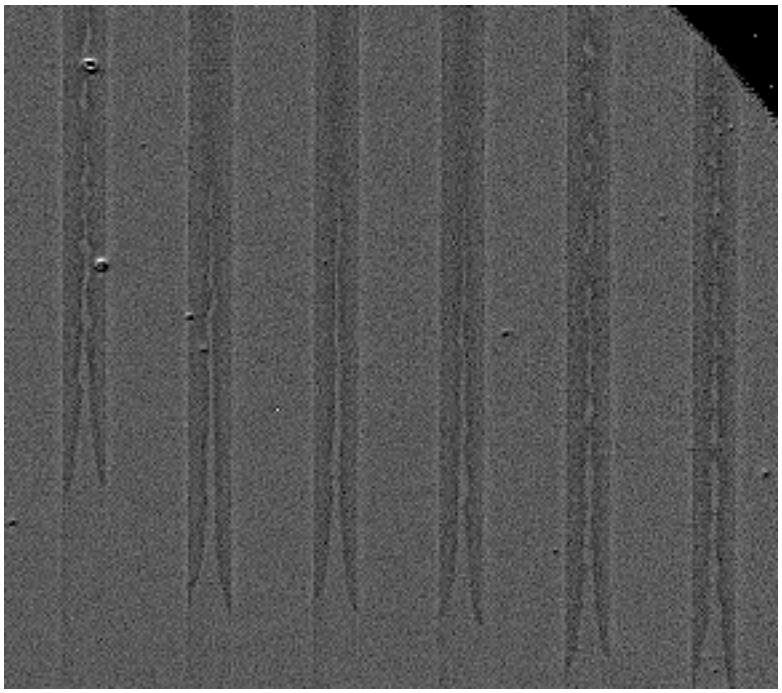

Figure 21: Image from a glass 57 nm channel exhibiting a parabolic cross-section etched from germanium with a 1 μm top wall thickness exhibiting a non-standard flow pattern with deionized water as the working fluid.

SEM analysis of a channel that had been originally fabricated with a 57 nm tall parallel plate geometry and a 1 μm thick channel top were obtained after introducing a liquid plug. The

images revealed that the resulting channel geometry was actually parabolic after experimentation with a channel center height of 261.3 nm, which is almost four and a half times the original manufactured channel height due to deflection of the thin silicon dioxide top channel wall (Fig. 22). The channel height during filling may be even smaller than the height dimension captured at the end of the experiment due to the large negative transient capillary pressures exerted by a dynamic liquid plug confined within the channel walls. Therefore, constructing nanochannels with top wall thicknesses < 3 μm may result in significant channel deformation and an altered flow profile.

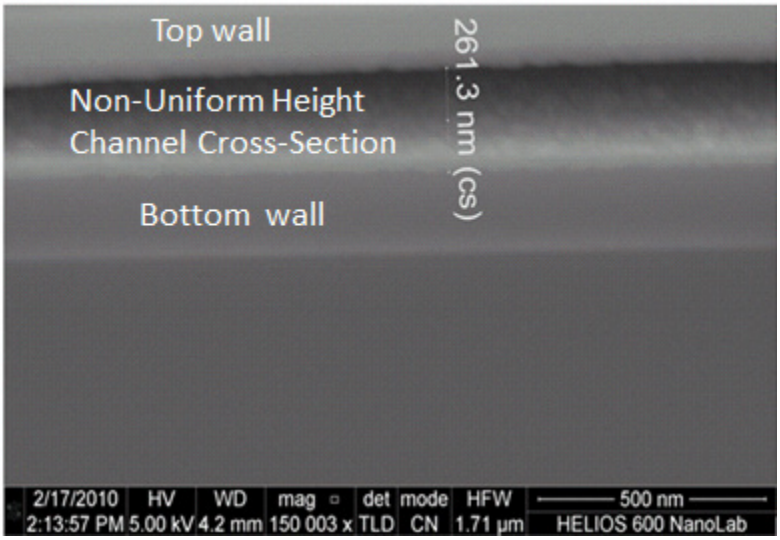

Figure 22: Scanning electron microscope image of a glass channel exhibiting a parabolic cross-section with a 1 μm top wall thickness with the wall-to-wall spacing of 57nm near the edges to 261.3 nm near the channel center.

Application of the modified Washburn equation to describe the non-standard flow in a parabolic nanochannel was attempted but did not accurately predict the experimental results. Figure 23 reports the modified Washburn prediction for varying wall-to-wall spacing channels and experimentally observed meniscus locations squared as a function of time.

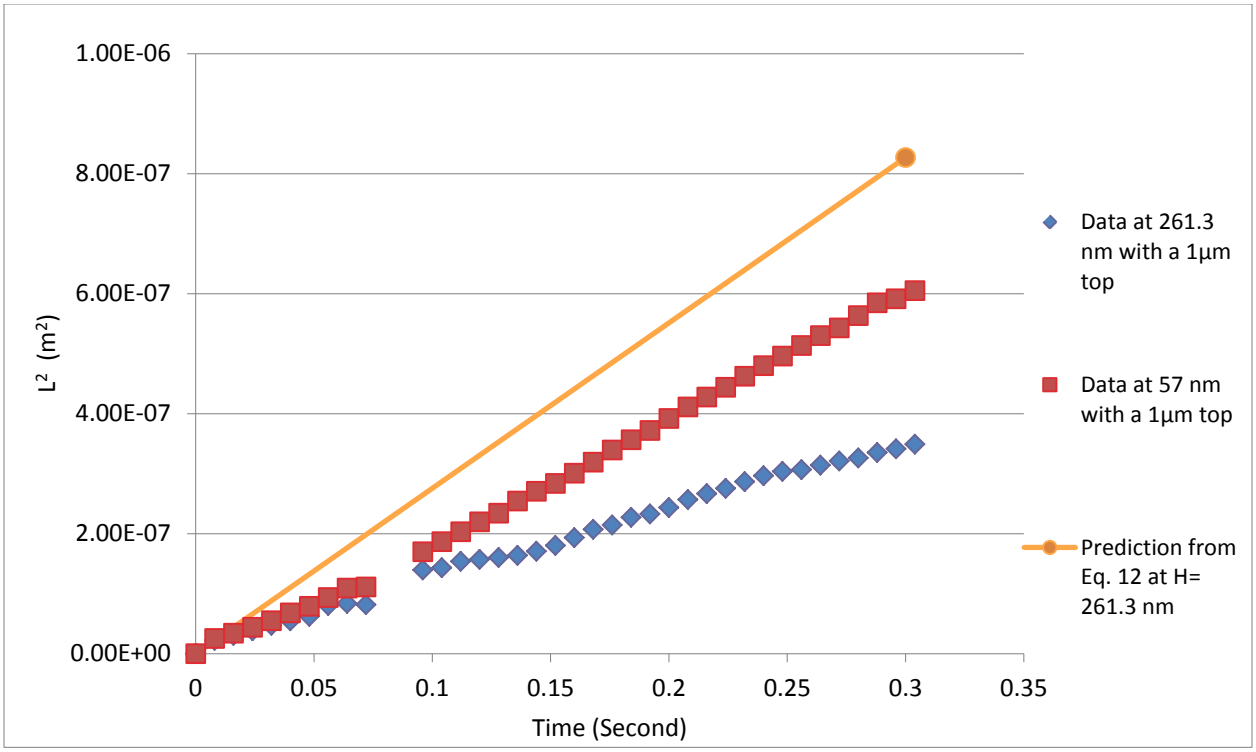

Figure 23: Square of the meniscus location vs. time for glass channels exhibiting a parabolic cross-section etched from germanium sacrificial cores with a 1 µm top wall thickness with the wall-to-wall spacing of 57 nm to 261.3 nm and with deionized water as the working fluid.

The advancing contact angle utilized for the calculations in Figure 23 was 17.5 degrees, which was the average value observed in the 7 µm and 5 µm parallel plate channel experiments. The effective height value, 185.5 nm, was calculated from the analytical model developed in this study, Eq. 12. The resulting modified Washburn prediction of the meniscus location was 32.5% higher than the experimental filling rate. This large discrepancy may be due to the difference in the channel height during the actual filling and the measured channel height at the end of the experiment. In order to obtain an accurate height measurement during filling, an *in situ* measurement is needed. If the channel height during is filling is larger than that measured at the conclusion of the experiment, then the model could be adequate for the description of flow in a parabolic nanochannel. For example, if the actual height of the parabolic channel during filling, H_{max} and H_B from Eq. 17, were 105 nm, respectively, then using the modified Washburn

prediction, the error would be reduced to zero percent. The leading edges of the experimental flow correspond to the 57 nm tall height data. The center height corresponds to the 261.3 nm data. The resulting slope of the square of the meniscus location as a function of time from linear regression analysis is shown in Table 15 compared to the theoretical prediction of the modified Washburn equation using the channel height from the cross-section in the SEM measurements.

Table 15: Parabolic Summary – Deionized Water in a 57 to 261.3 nm Channel

Height	Modified Washburn Theory Slope L_{eff}^2	Linear Regression Experimental Slope	Nominal Deviation from Theory
µm	mm^2/second	mm^2/second	Percent
261.3	0.816 ± .078	1.21 ± .043	32.5

The meniscus distortion equation, Eq. 22, compares the experimental meniscus distortion based on the ratio of channel heights and the distance from the channel entrance. Applying a correction factor of 0.32 to the meniscus distortion model gives an error of 314.0% as seen in Figure 24; however, this assumes the correctional factor for a nanoscale parabolic and a microscale tapered channel are the same. A correctional factor of 0.08 results in nominally zero deviation from the experimental data. The 57 nm height data was curve fit prior to comparison of the meniscus distortion prediction in order to decrease experimental noise.

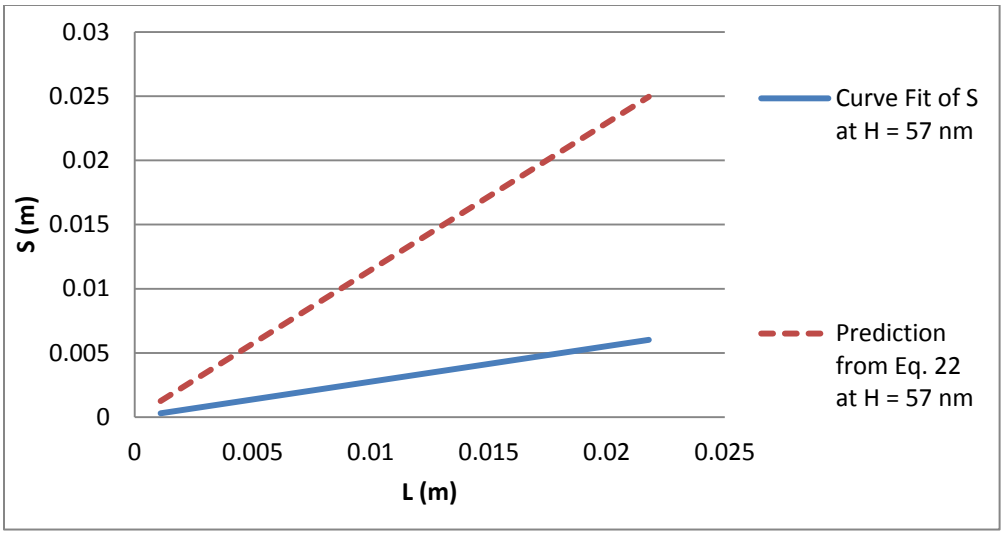

Figure 24: Predicted meniscus locations are compared to actual deionized water meniscus locations for a parabolic nanochannel where 261.3 nm was determined to be the tallest height.

It is unknown whether the tapered correctional coefficient, *C,* from Equation 22, is the same for a nanoscale parabolic bowed channel. More experimentation on alternate channel sizes is needed to determine an accurate correctional coefficient for nanoscale parabolic channels.

4.5 Nanoscale Filling Rate Measurements

The experimentally determined square of the meniscus location versus time values from several other researchers are plotted together with the Washburn equation and the experimental results described herein in Figure 25 [5, 6, 8, 13, 17, 18, 19, 20, 21]. This shows a strong correlation between the flow rate predicted by the Washburn equation and the channel heights; however, there is considerable error for channel heights less than 60 nm, which can be attributed to a changing advancing contact angle, based on the channel height, that has not been accounted for in other research or from channel bowing during filling experimentation.

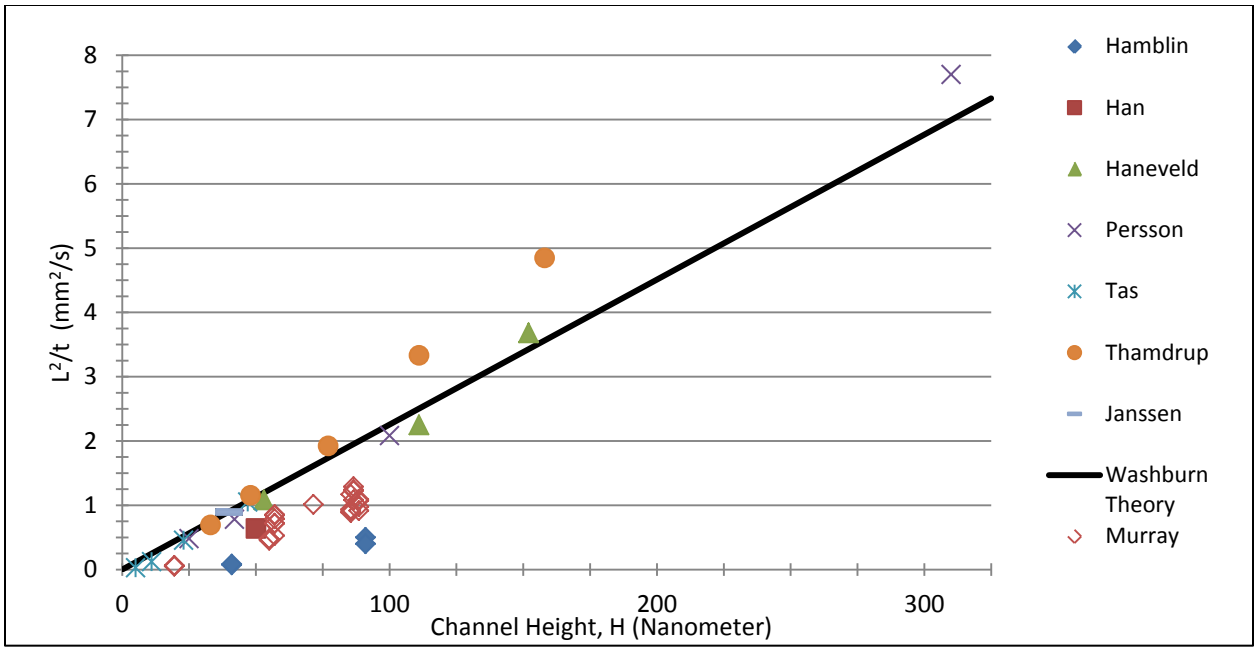

Figure 25: Overall experimental meniscus filling rates with deionized water

A number of generalizations and assumptions must be made in order to make such a broad comparison. First, the L^2/t values reported by previous researchers detailed the use of a macroscale advancing contact angles near 18 degrees regardless of channel height. Han, Haneveld, Tas, and Hamblin reported the advancing contact angle values in their respective work [5, 6, 8, 21]. A value of 20 degrees was assumed for the remaining research entries shown above [13, 17, 18, 19, 20]. The resulting error from the Washburn theory can partially be explained by the linearly decreasing advancing contact angle as the channel height decreases. Channel bowing may also contribute to the errors seen at nanoscale channel heights.

Figure 26 shows the percent error from the Washburn equation to emphasize the deviation between theoretical L^2/t from the classical Washburn equation and the experimental L^2/t values obtained through channels less than 80 nm tall when predicting the meniscus location over time.

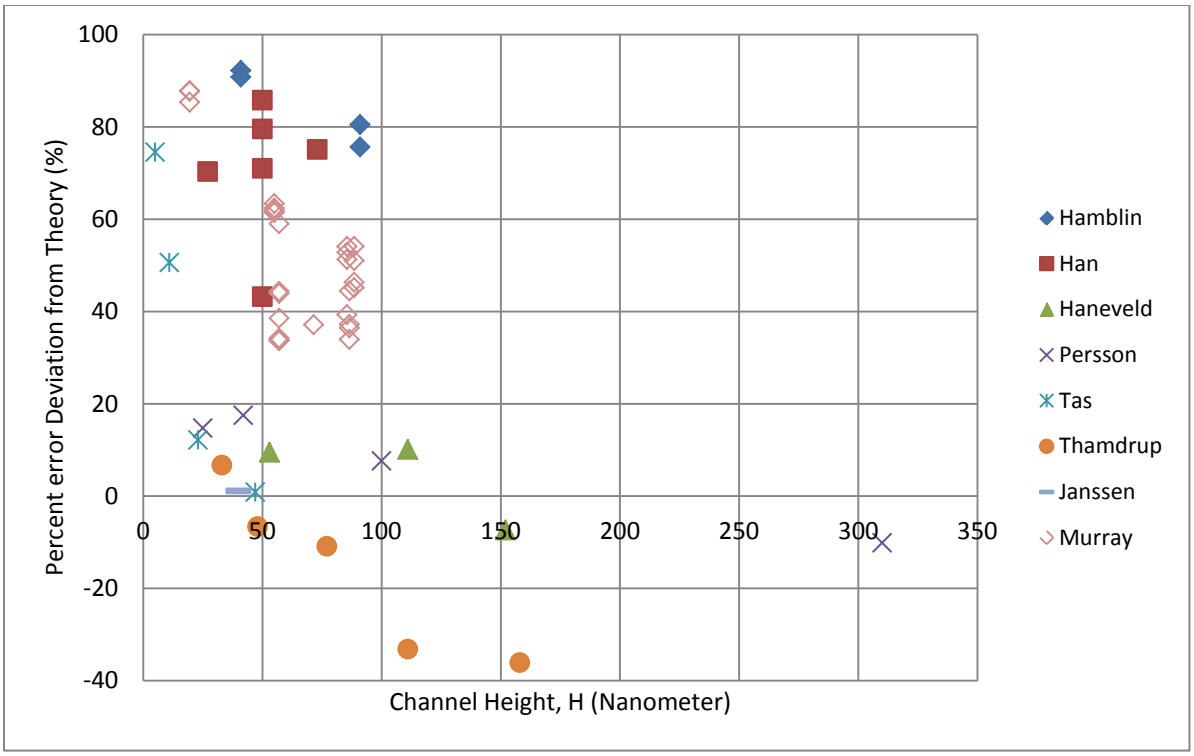

Figure 26: Nanochannel research percent error from the Washburn equation

Adjusting the advancing contact according to channel height leads to significant decreases in the experimental error for channel filling. The magnitude of contact angle adjustments increases with decreasing channel heights. Adjusting the contact angle to match the experimentally determined advancing contact angle can account for most of the error experienced at lower heights. For example, an error of 80% at 19.5 nm as seen in Figure 26, would be reduced to an error of 0.9% with application of the advancing contact angle which increases with decreasing channel height. Hamblin et al. also made reference to the contact angle changing based upon the nanometer channel height [21]; however, no correlation to channel height was attempted.

Figure 27 shows a curve fit for adjustment needed in static contact angle versus channel height. It demonstrates the results of experimentally solving for the advancing contact angle in

parallel-plate channels. The curve fit is valid for sacrificially etched channels with the same contact angle on each of the four walls. A modified slope may be needed for thermoformed channels since the contact angle filling rate behavior may deviate from sacrificially etched channels due to different wall materials. An asymptote may exist at heights near zero, and where the modification should asymptotically reach 90 degrees as the channel height approaches zero. The correlation would also asymptotically reach the macroscale advancing contact angle at a larger unknown channel height. Aluminum, chromium, and germanium channels were included in the advancing contact angle correlation.

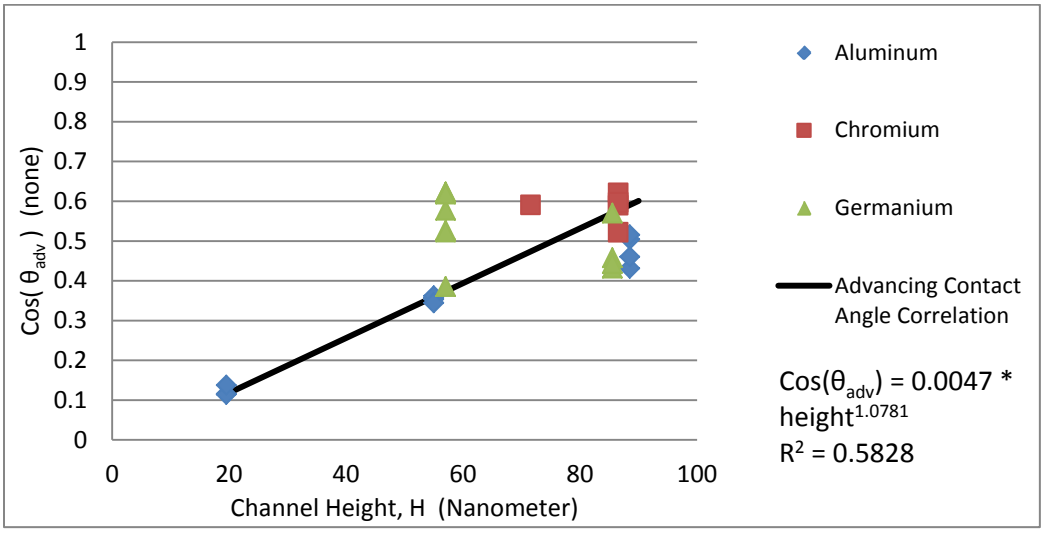

Figure 27: Curve fit for advancing contact angle adjustment for sacrificially etched nanochannels

The increase in deviation as channel height decreases indicates the changing contact angle based on channel height as the other fluid constants remain the same. The contact angle is suspect due to the small, confined channel width. The large negative capillary pressure must force the contact angle to change in order to satisfy both wall constraints.

5 CONCLUSIONS AND FUTURE WORK

Quantification and prediction of capillary fluid flow in micro- and nanochannels continues to contribute to the development of many emerging technologies. The Washburn equation has been developed to predict flow in parallel-plate channels; however, current nanofabrication processes may produce nanochannels with non-planar wall spacing. Furthermore, microscale channels with different cross-sections (i.e. taper) could have different filling properties that may expand the range of microfluidic applications. These variations in wall spacing affect the transient dynamics of a liquid plug filling the channel, causing deviations from the classical behavior of a parallel-plate system.

Filling of microscale parallel-plate channels was performed to obtain a calculated advancing contact angle, which were employed in the tapered microscale channel filling experiments. Tapered microscale channel filling slope values were opposite of the expected trend given from the Washburn equation. At taller channel heights, the meniscus filling slope decreased, whereas at lower channel heights L^2/t values were elevated.

A modified Washburn equation that utilizes an effective height to predict the filling speed corresponding to the location of the tallest height within a channel was derived and validated experimentally in both tapered microscale channels and nanoscale parabolic channels with three different fluids. Channel effective height calculations regarding tapered channel flow for methanol and isopropanol fluids are recommended, as the error between experimental and

theoretical filling L^2/t values were low. Parallel-plate nanochannel experimentation showed the advancing contact angle either remaining the same, or decreasing relative to the static contact angle in all calculations. Observations and conclusions made during experimentation and analysis have been organized in this chapter by decreasing channel height. Parallel-plate observations precede tapered and parabolic conclusions.

Future work ideas are also documented in order to further understand the large deviation between theory and experimental values such as extra experimentation to hone in on the correct advancing contact angle based on channel height for deionized water in tapered filling scenarios.

5.1 **Microscale Parallel-Plate Channels**

Acrylic microscale parallel-plate channels were constructed, thoroughly characterized using a profilometer, and filled with three different fluids. The advancing contact angles for methanol, isopropanol, and deionized water were accurately determined. However, the value of the inverse cosine of the advancing contact angle for methanol and isopropanol was greater than one, so the advancing contact angle was assumed to be zero. This could be caused by a number of factors. Large channel height variations were observed with the acrylic plates; the channel height was approximately 70 μm greater at the channel exit than at the channel entrance. The surface tension value for each fluid was determined experimentally but deviated from tabulated values. Dynamic viscosity was interpolated from tabulated values based on temperature instead of being measured directly. Errors in either of these variables would affect the calculation of the inverse cosine of the advancing contact angle and could be corrected through additional experimentation.

5.2 Microscale Channel Taper Theory Development

The filling of microscale tapered channels was measured and compared to theoretical predictions based on the modified Washburn equation. Experimentation with methanol and isopropanol demonstrated that employing an effective channel height is an effective method for correctly calculating the square of the meniscus position as a function of time for the largest channel height (see Sections 4.2.1 and 4.2.2). The effective channel height correlation successfully determined the overall average flow rate for methanol and isopropanol, including an accurate prediction of the experimental observation that the filling slope is greater for smaller channel heights and lower for larger channel heights. Of course, the success of the modified Washburn equation was dependent on the determination of the advancing contact angle from the parallel-plate experimentation described above.

The filling of tapered channels with deionized water was more complicated. As the parallel-plate advancing contact angle adjustment should have accounted for the only changing fluid constant, the large observed experimental errors indicated that a change in flow had occurred within the tapered channel. A result of the secondary flow was a reversal of the expected experimental filling slope characteristics relative to methanol and isopropanol. Comparing the effective height filling values to the average height filling values may be a better solution in the interim before a new flow model can be derived in order to predict filling values for tapered channels that exhibit a secondary flow.

5.3 Nanoscale Filling Rate Measurements

Aluminum, chromium, and germanium parallel-plate channel filling experiments were performed with different channel heights and surface treatments. The results for all channels with top wall thicknesses greater than 3 μm showed good agreement with theoretical prediction.

Correcting the advancing contact angle greatly improves the accuracy of filling predictions using the Washburn equation, especially in nanochannels with heights less than 60 nm. Assuming the contact angles of the fluid on all four channel surfaces were the same since each side was thermally deposited onto the channel, more experimentation should be carried out to correlate the change in advancing contact angle with channel height. In order to more fully correlate the change in advancing contact angle for deionized water, additional testing of channels with heights less than 20 nm, near 40 nm, and 100 nanometers with sacrificially etched nanochannels is needed. A normalized theory could be extended to other fluids of interest once deionized water, methanol, and isopropanol correlations are finalized.

5.4 **Nanoscale Parabolic Channel Filling Rate**

Nanochannels with top wall thicknesses less than 3 μm show significant deviations from classical theoretical predictions. Characterization of germanium etched 57 nm channel with a 1 μm top wall by SEM revealed deformation of the channel with a resulting parabolic shape. The extremely large deviations from the expected theoretical filling rates described herein are similar to the observations made by other researchers of nanochannels that were believed to be parallel-plate channels [17]; however, the observations and results from the parabolic channels have revealed the involvement of non-planar channels. The effective channel height correlation was able to explain the overall deviation from theory as it over estimated the filling slope values based on the advancing contact angle adjustment. It also confirmed the visual results obtained with the 57 nm channel with the 3 μm top, which also reduced the overall flow rate, and the 57 nm channel with a 1 μm top. The effective channel height correlation, in this instance, would benefit from an *in situ* measurement of the channel height as the liquid remains in the channel as the large pressures are suspect to force more bowing than was measured via SEM.

5.5 **Future Work**

A mathematical model for the capillary filling of tapered channels with a changing cross section throughout the length of the channel could be derived in order to correctly predict fluid flow through any combined cross sections for a given, well-quantified channel height and the resulting fluid flow. Future work should entail deriving an analytical model including a transverse pressure gradient within tapered channel heights to correctly predict the change in the L^2/t values experienced throughout this study. Other work might entail particle image velocimetry, which could be used to confirm the existing flow gradient from the taller channel section to the lower height section.

REFERENCES

1. Douville N, Huh D, & Takayama S (2008) DNA linearization through confinement in nanofluidic channels. *Analytical and bioanalytical chemistry*, *391*(7), 2395-2409.

2. Hamblin MN, Xuan J, Maynes D, Tolley HD, Belnap DM, Wooley AT, Lee ML, Hawkins AR (2009) "Selective trapping and concentration of nanoparticles and viruses in dual height nanofluidic channels," *Lab on a Chip,* 10:173-178.

3. Eijkel JCT and van de Berg A (2005) "Nanofluidics: What is it and what can we expect from it," *Microfluid and Nanofluid* 1:249-267.

4. Solobev VD, Churaev NV, Velarde MG, and Zorin ZM (2000) "Surface tension and dynamic contact angle of water in thin quartz capillaries," *J. Coll. Int. Sci.* 222:51-54.

5. Haneveld J, Tas NR, Brunets N, Jansen HV and Elwenspoek M (2008)"Capillary filling of sub-10 nm nanochannels," *J. App. Phys.* 104:014309.

6. Tas NR, Haneveld J, Jansen V, Elwenspoek M, van den Berg A (2004) "Capillary filling speed of water in nanochannels," *App. Phys. Lett.* 85:3274-3276.

7. Hibara A, Saito T, Kim HB, Tokeshi M, Ooi T, Nakao M, and Kitamori T (2002) "Nanochannels on a fused-silica microchip and liquid properties investigation by time-resolved fluorescence measurements*," Anal. Chem*. 74:6170-6176.

8. Han A, Mondin G, Hegelbach NG, do Rooij, JF, Staufer UJ (2006) "Filling kinetics of liquids in nanochannels as narrow as 27 nm by capillary force," *J. Colloid Int. Sci.* 293:151-157.

9. Judy J, Maynes D, and Webb BW (2002) "Characterization of frictional pressure drop for liquid flows through microchannels," *Int. J. Heat Mass Trans.* 45:3477-3489.

10. Woolford B, Maynes D and Webb BW (2009) “Liquid Flow Through Microchannels with Grooved Walls Under Wetting and Superhydrophobic Conditions,” *Microfluid and Nanofluid*, In Press.

11. Washburn EW (1921) “The dynamics of capillary flow*,”Phys. Rev.* 17:273-283.

12. Mortensen NA and Kristensen A (2008) “Electroviscous effects in capillary filling of nanochannels,” *App. Phys. Lett.* 92:063110.

13. Thamdrup LH, Persson F, Bruus H, and Kristensen A (2007) Experimental investigation of bubble formation during capillary filling of SiO_2 slits, *App. Phys. Lett.* 91:163505.

14. Israelachvili JN (1986) “Measurement of the viscosity of liquids in very thin films,” *J. Colloid Interface Sci.,* 110:263-271.

15. Honschoten JW, Escalante M, Tas NR, Jansen HV, Elwenspoek M (2007) “Elastocapillary filling of deformable nanochannels,” *J. of Applied Physics* 101 (9):94310-94310-7.

16. Honschoten JW, Escalante M Tas NR, Elwenspoek M (2008) “Formation of liquid menisci in flexible nanochannels,” *J. Colloid Interface Sci.*, 329 (1):133-139.

17. Honschonten JW, Brunets N, Tas NR (2010) “Capillarity at the nanoscale,” *Chemical Society Review*, 39:1096-1114.

18. Tas NR, Escalante M, Honschoten JW, Jansen HV, Elwenspoek M (2010) “Capillary Negative Pressure measured by Nanochannel Collapse,” *American Chemical Society*, 26 (3):1473-1476.

19. Peng-Fei H, Feng H, Ke-Qin Z (2005) “Flow characteristics in a trapezoidal silicon microchannel,” *J. Micromech Microeng,* 15:1362.

20. Zhu Y, Petkovic-Duran K (2006) “Capillary flow in polymer microfluidic chips,” *Proc. SPIE,* 6416:64160K.

21. Hamblin MN, Hawkins AR, Murray D, Maynes D, Lee ML, Woolley AT, Tolley D (2011) “Capillary flow in sacrificially etched nanochannels,” *Biomicrofluidics*, 5:021102.

22. Goodwin RD (1987) “Methanol Thermodynamic Properties From 176 to 673 K at Pressures to 700 Bar,” *Journal of Physical and Chemical Reference Data*, 16:799

23. Lange, NA. *Lange’s Handbook of Chemistry*. New York: McGraw-Hill, 1973. Print.

24. Lide, DR. *CRC Handbook of Chemistry and Physics*. Florida: CRC Press, 2004. Print.